Universidad de Cantabria

Facultad
de
Ciencias

Estudio de transiciones de Peierls en un metal unidimensional

Study of Peierls' transitions in a one-dimensional metal

Trabajo de Fin de Grado
para acceder al

GRADO EN FÍSICA

Autor: José Blanco Herrera

Director: Javier Junquera

Junio - 2024

Acknowledgements

I would like to express my gratitude to the following people for their support and guidance throughout the completion of this work:

Firstly, I would like to thank Nayara, Toraya and Inés for their help with the use of SIESTA and the functioning of some of its internal mechanisms.

I am also deeply grateful to Pablo, who helped me immensely with some of the mathematical concepts of vital importance developed in this work.

My sincere thanks to Lucía and Adriana for their unwavering moral support and for always believing in my abilities and potential. Their patience and understanding during the most demanding times have been invaluable.

Lastly, I wish to thank Javier, the supervisor of this work, for his interest and the effort put into ensuring that this work progresses in the best possible way, making this an enriching experience.

Resumen

El teorema de Peierls establece que cualquier cadena unidimensional con los átomos equidistantes entre sí es inestable respecto de una deformación de la red que elimine la degeneración en el nivel de Fermi. Este tipo de distorsión viene caracterizada por un fonón en el borde de la primera zona de Brillouin, en última instancia, la dimerización de la cadena: los átomos se disponen en pares, dando lugar a enlaces largos y cortos. Esta transición surge de la competencia entre las dos componentes energéticas principales de los sistemas sólidos: la electrónica y la elástica. La energía electrónica se ve reducida por la dimerización, contrariamente a la elástica.

En este trabajo se ha desarrollado un modelo teórico analítico en el que se profundiza en las características electrónicas y de red de una cadena monoatómica unidimensional, estudiando ambas componentes de forma independiente para posteriormente acoplar la interacción electrón-red y analizar la competencia entre las mismas, comprobando así el teorema de Peierls y analizando las características de la dimerización: la ganancia energética, el desplazamiento de los átomos de la red, la apertura del gap y la densidad de estados.

Posteriormente, se llevan a cabo simulaciones computacionales desde primeros principios con SIESTA, en las que se analiza esta transición con un modelo profundo y robusto basado en la teoría del funcional de la densidad (DFT, por sus siglas en inglés). Adicionalmente, se va a someter a la cadena unidimensional a una serie de potenciales externos que modifican la intensidad de las interacciones dentro de la red y, por tanto, las características de la dimerización, para estudiarlas en diferentes regímenes. Finalmente, se integran ambos modelos teóricos para su consiguiente comparación, analizando sus diferencias y la validez del modelo analítico.

Palabras clave: Peierls, dimerización, transición, unidimensional, SIESTA, primeros principios, enlace fuerte.

Abstract

The Peierls theorem states that any one-dimensional chain with equidistant atoms is unstable with respect to a lattice deformation that lifts up the degeneracy at the Fermi level. This distortion is characterized by a phonon at the edge of the 1^{st} Brillouin zone, ultimately leading to the dimerization of the chain: atoms arrange into pairs (dimers), thereby forming long and short bonds. This transition arises from the competition between the two primary energy components of solid systems: electronic and elastic. Electronic energy is reduced by the dimerization, contrary to the elastic energy.

In this study, a theoretical analytical model has been developed to delve into the electronic and lattice characteristics of a one-dimensional monoatomic chain, investigating both components independently and subsequently coupling the electron-lattice interaction. This allows the analysis of their interplay, leading to the verification of the Peierls theorem and the study of the characteristics of the dimerization: the energy gain, the atomic displacements, the gap opening, and the density of states.

Besides, first-principles computational simulations are carried out with SIESTA, which allows the study of this transition within a comprehensive framework: the density functional theory (DFT). Additionally, the one-dimensional chain is subjected to various external potentials altering the lattice interactions and thereby dimerization characteristics across different regimes. Finally, both theoretical models are combined for a comparative analysis, evaluating the differences and the validity of the analytical model.

Key words: Peierls, dimerization, transition, one-dimensional, SIESTA, first-principles, tight-binding.

Contents

1 Historical background and motivation

Rudolf Ernst Peierls, from now on, Peierls, is recognized as a significant figure in 20th-century theoretical physics, particularly in the realm of Solid State Physics, now termed Condensed Matter Physics. Born on June 5, 1907, in a suburb of Berlin, Peierls initially aspired to pursue engineering. However, due to the fact that he "was rather clumsy" with his hands [1], he decided to pursue Physics studies instead. His career has been marked by several great physicists of the time, such as Sommerfeld, Heisenberg, Bloch, Pauli, and many more. His academic trajectory has been profoundly connected to Solid State Physics. He began his journey in this field when he attended some lectures imparted by Heisenberg in Leipzig during his stay in 1928, where he met Felix Bloch, a scientist from whom he "benefited greatly" [1]. In Leipzig, Peierls delved into an investigation of the anomalous Hall effect under Heisenberg's guidance, which subsequently led to him joining Wolfgang Pauli in spring of 1929 at the ETH in Zurich, where he embarked on investigations into the vibrations of atom within crystal lattices, that he later synthesized into his thesis. Later on, he became Pauli's student, and worked with other great figures like Lev Landau. In Peierls' words, the 1920s were "an exciting time in Physics" [1], given the rise of the new Physics.

Peierls belonged to the first generation of physicists to make use of the Quantum Theory, specially in the 1930s, after he decided to emigrate to England in order to escape from the Nazi Germany [1]. Anyway, Peierls did not focus his studies in Solid State Physics during that time, even though he kept working as a theoretical physicist, slightly focused on quantum electrodynamics and quantum field theory. He would consider himself as a generalist, a person that "learns less and less about more and more until he knows nothing about everything" [1]. It was not until 1953, when he gave a course of lectures on Solid State Physics at the summer school at Les Houches, that he realized that most of the problems within this field that he had regarded as open questions fifteen years earlier were still unsolved, and he decided to go back to them, in particular to those related to the theory of conductivity.

The classes Peierls imparted in 1953 "required, for once, written lecture notes", which he decided to turn into a book [1], called Quantum Theory of Solids. In the words of David Mermin, in his autobiography [2]: "It was beautifully written, much more thoughtful and coherent than any of the few existing texts". The next quotation, extracted directly from Peierls' autobiography "Bird of Passage: Recollections of a Physicist" [1], regarding his book about Solid State Physics, is crucial for this work:

> "In the course of tidying up the material for my book, I looked carefully at the way the atoms in a metal crystal hang together, partly as a result of the almost free electrons moving between them. I noticed that in one dimension, i.e., in a linear chain, the periodic structure, with all distances between adjacent atoms equal, is not stable and will always suffer some distortion. This seemed at first a very bizarre result, and I wondered whether there was a flaw in my reasoning. I put my argument to Maurice Pryce, then in Oxford and one of the most critical theoreticians I know, but he could not see anything wrong. So I put the argument in my book. It seemed an academic point, as there are no one-dimensional metals in nature. Some twenty years later, when experiments on nearly one-dimensional organic crystals, in which molecules are arranged in long chains, showed a novel type of transition, my old result was remembered. The "Peierls transition" or "Peierls instability" has now become a standard term."

Where it can be seen that the so-called Peierls' transition was first mentioned in his book, just as a result. Nowadays, it is perceived as a theorem, which states that any linear chain with equidistant atoms is unstable. To be precise, it is unstable with respect to a lattice distortion that lifts up the degeneracy at the Fermi level [3]. This instability arises from the competition between the two main energy components of the system: the electronic and the elastic contributions. From an electronic perspective, the system is energetically favored

when it dimerizes, alternating short (strong) and long (weak) bonds. Conversely, from an elastic standpoint, the dimerized configuration is inherently unstable, and the system tends to revert to the equidistant state. Peierls instability manifests when the electronic energy component dominates, leading to the dimerization of the system despite the opposing elastic forces. Upon dimerization, the electronic band structure of the system is altered. A gap emerges at the edge of the first Brillouin zone, separating the valence and conduction bands, and therefore lifting the degeneracy at the Fermi level. This results in a reduction of the system's electronic energy, giving place to a metal-insulator transition.

Initially, in this work we will conduct an analytical study of a monoatomic linear chain composed of Hydrogen atoms [Sec. 2.2]. The model will assume an orthogonal basis of s-symmetry orbitals, one per site, and will restrict interactions to nearest neighbors. The electronic properties will be treated using the tight-binding model [Sec. 2.1], while the elastic properties will be analyzed using phonon theory [Sec. 2.3]. Furthermore, the electron-lattice coupling will be studied to understand the interplay between electronic and elastic components of the system [Sec. 2.4]. Subsequently, the complexity of the model will be increased. The orthogonality of the orbitals will be removed, and interactions will be extended beyond nearest neighbors for both electronic and lattice components. To achieve this, first-principles numerical simulations will be performed using SIESTA [4] [Sec. 3]. Finally, the two models will be quantitatively compared, extracting parameters for the simplified analytical model from the first-principles atomistic simulations [Sec. 3.4].

Peierls instability serves as an example that band theory is an insufficient model to explain some of the interesting phenomena occurring within Solid State Physics. If only band theory is considered to analyze a one-dimensional monoatomic chain, it predicts that the system behaves like a metal, being its most stable configuration the one with equidistant atoms, which, as will be demonstrated throughout this work, is not true. There are other phenomena that produce metal-insulator transitions that take place when more sophisticated treatments are done, going beyond simple band theory, such as the Jahn-Teller distortion [5], [6], [7], the Crystal-Field splitting [8], and the magnetic ordering [9], [10].

Besides, this instability is not merely a theoretical phenomenon. There are compounds, such as polymer chains forming rings, that exhibit the Peierls distortion. In fact, this case is of great interest due to the possibility of modulating the transition by varying the magnetic flux through the ring [11]. Another example of a compound that exhibits the Peierls transition is the Au-induced atomic wire array on a stepped Si(553) surface, which actually shows two simultaneous distortions with different periodicities and transition temperatures. These transitions have been observed through angle-resolved photoemission [12]. Besides, since this phenomena imply the rearrangement of the ions in solid systems, it produces fluctuations in the electronic density, known as charge density waves (CDW). Materials such as $NbSe_2$ and $K_{0.3}MoO_3$ exhibit these CDW [13]. This transition finds applications in fields such as nanotechnology [14], [15], superconductivity [16], [17], and quantum computing [18].

From an academic perspective, this work requires knowledge and application of various areas within Physics and Mathematics, integrated throughout its development. Fundamental areas include Condensed Matter Physics, core to this study, Quantum Mechanics (theory of atomic orbitals, resolution of the time-independent Schrödinger equation, eigenvalues of the Hamiltonian operator...), Computational Physics, Classical Mechanics (theory of elasticity and oscillatory motion), Differential and Integral Calculus, among others.

2 Theoretical analytical model

2.1 Brief revision of the tight-binding approach

2.1.1 A basis set of atomic orbitals

Let's start our discussion with a set of local orbital basis $\phi_\alpha(\vec{r}-\vec{R}_I)$, each associated with an atom in the unit cell at position $\vec{R}_I$.

In principle, α might run over all the atomic orbitals of a given atom ($1s$, $2s$, $2p$, $3d$, ...). In practice, we shall restrict the atomic orbitals that will be explicitly included in the simulation to a given subset, typically only the atomic orbitals that participate in the description of the states at the energy window of interest are retained. In order to simplify the notation, we will let μ denote both α and the site I, so that μ runs from 1 to N_{basis} (the total number of atomic orbitals retained in the basis set in a unit cell). With this new notation, the atomic orbital can also be written as $\phi_\mu(\vec{r}-\vec{R}_\mu)$. In a crystal, the atoms in a unit cell are at positions $\vec{\tau}_{\kappa,j}$, where $\vec{\tau}_{\kappa,j}$ is the position of the $j=1,\ldots,n_\kappa$ atoms of type κ. The composite index $\{\kappa,j,\alpha\rightarrow\mu\}$ allows the entire basis to be specified by $\phi_\mu\left[\vec{r}-\left(\vec{\tau}_\mu+\vec{T}\right)\right]$, where $\vec{T}$ is a translation vector of the Bravais lattice.

We know that the eigenstates of a Hamiltonian in a periodic potential must comply with the Bloch theorem,

$$\psi_{n\vec{k}}(\vec{r}) = e^{i\vec{k}\cdot\vec{r}}u_{n\vec{k}}(\vec{r}), \tag{1}$$

where n is a band index, $\vec{k}$ is a wavevector in the first Brillouin zone, and $u_{n\vec{k}}(\vec{r})$ is a function with the periodicity of the Bravais lattice.

$$u_{n\vec{k}}(\vec{r}) = u_{n\vec{k}}(\vec{r}+\vec{T}). \tag{2}$$

As a corollary of the Bloch theorem, we can also state that

$$\psi_{n\vec{k}}(\vec{r}+\vec{T}) = e^{i\vec{k}\cdot\vec{T}}\psi_{n\vec{k}}(\vec{r}). \tag{3}$$

A good starting point to represent the eigenstate $\psi_{n\vec{k}}(\vec{r})$ in a basis of localized atomic orbitals is to define a basis that complies also with the Bloch theorem, i.e. by defining a basis state with wavevector $\vec{k}$

$$\phi_{\mu\vec{k}}(\vec{r}) = A_{\mu\vec{k}}\sum_{\vec{T}} e^{i\vec{k}\cdot\vec{T}}\phi_\mu(\vec{r}-\vec{\tau}_\mu-\vec{T}). \tag{4}$$

where $\vec{\tau}_\mu$ is the position of the atom within the unit cell to which orbital ϕ_μ belongs, and $A_{\mu\vec{k}}$ is a normalization factor.

2.1.2 The Hamiltonian matrix elements

The next step is the computation of the Hamiltonian matrix elements in these basis of numerical atomic orbitals. From the expressions given in Eq. (4)

$$\begin{aligned}\langle\phi_\mu(\vec{k})|\hat{H}|\phi_\nu(\vec{k}')\rangle &= A^*_{\mu\vec{k}}\sum_{\vec{T}} e^{-i\vec{k}\cdot\vec{T}}\int_{\text{all space}}\mathrm{d}\vec{r}\phi^*_\mu(\vec{r}-\vec{\tau}_\mu-\vec{T})\hat{H}\left(A_{\nu\vec{k}'}\sum_{\vec{T}'}e^{i\vec{k}'\cdot\vec{T}'}\phi_\nu(\vec{r}-\vec{\tau}_\nu-\vec{T}')\right)\\ &= A^*_{\mu\vec{k}}A_{\nu\vec{k}'}\sum_{\vec{T}}\left(\sum_{\vec{T}'}e^{i\left(\vec{k}'\cdot\vec{T}'-\vec{k}\cdot\vec{T}\right)}\int_{\text{all space}}\mathrm{d}\vec{r}\phi^*_\mu(\vec{r}-\vec{\tau}_\mu-\vec{T})\hat{H}\phi_\nu(\vec{r}-\vec{\tau}_\nu-\vec{T}')\right).\end{aligned} \tag{5}$$

In the sum in brackets, the translation vector $\vec{T}$ is fixed. We can therefore make the following change of variables in the integral $\vec{r}' = \vec{r} - \vec{T}$,

$$\begin{aligned}\langle\phi_\mu(\vec{k})|\hat{H}|\phi_\nu(\vec{k}')\rangle &= A^*_{\mu\vec{k}}A_{\nu\vec{k}'}\sum_{\vec{T}}\left(\sum_{\vec{T}'}e^{i\left(\vec{k}'\cdot\vec{T}'-\vec{k}\cdot\vec{T}\right)}\int_{\text{all space}}\mathrm{d}\vec{r}'\,\phi^*_\mu(\vec{r}'+\vec{T}-\vec{\tau}_\mu-\vec{T})\hat{H}\phi_\nu(\vec{r}'+\vec{T}-\vec{\tau}_\nu-\vec{T}')\right)\\ &= A^*_{\mu\vec{k}}A_{\nu\vec{k}'}\sum_{\vec{T}}\left(\sum_{\vec{T}'}e^{i\left(\vec{k}'\cdot\vec{T}'-\vec{k}\cdot\vec{T}\right)}\int_{\text{all space}}\mathrm{d}\vec{r}'\,\phi^*_\mu(\vec{r}'-\vec{\tau}_\mu)\hat{H}\phi_\nu\left[\vec{r}'-\vec{\tau}_\nu-\left(\vec{T}'-\vec{T}\right)\right]\right).\end{aligned} \tag{6}$$

Now, making the change in variables $\vec{T}' - \vec{T} = \vec{T}''$,

$$\begin{aligned}\langle\phi_\mu(\vec{k})|\hat{H}|\phi_\nu(\vec{k}')\rangle &= A^*_{\mu\vec{k}}A_{\nu\vec{k}'}\sum_{\vec{T}}\left(\sum_{\vec{T}''}e^{i\left(\vec{k}'\cdot\left(\vec{T}''+\vec{T}\right)-\vec{k}\cdot\vec{T}\right)}\int_{\text{all space}}\mathrm{d}\vec{r}'\,\phi^*_\mu(\vec{r}'-\vec{\tau}_\mu)\hat{H}\phi_\nu(\vec{r}'-\vec{\tau}_\nu-\vec{T}'')\right)\\ &= A^*_{\mu\vec{k}}A_{\nu\vec{k}'}\left[\sum_{\vec{T}}e^{i\left(\vec{k}'-\vec{k}\right)\cdot\vec{T}}\right]\left(\sum_{\vec{T}''}e^{i\vec{k}'\cdot\vec{T}''}\int_{\text{all space}}\mathrm{d}\vec{r}'\,\phi^*_\mu(\vec{r}'-\vec{\tau}_\mu)\hat{H}\phi_\nu(\vec{r}'-\vec{\tau}_\nu-\vec{T}'')\right)\\ &= N\delta_{\vec{k},\vec{k}'}A^*_{\mu\vec{k}}A_{\nu\vec{k}'}\left(\sum_{\vec{T}''}e^{i\vec{k}'\cdot\vec{T}''}\int_{\text{all space}}\mathrm{d}\vec{r}'\,\phi^*_\mu(\vec{r}'-\vec{\tau}_\mu)\hat{H}\phi_\nu(\vec{r}'-\vec{\tau}_\nu-\vec{T}'')\right),\end{aligned} \tag{7}$$

where we have used Eq. (8a) [see Ref. [19], Eq. (F.4)]

$$\sum_{\vec{T}}e^{i\vec{k}\cdot\vec{T}} = N\delta_{\vec{k},\vec{0}}, \tag{8a}$$

$$\sum_{\vec{k}}e^{i\vec{k}\cdot\vec{T}} = N\delta_{\vec{T},\vec{0}}, \tag{8b}$$

where $\vec{T}$ runs through the N sites of the Bravais lattice in Eq. (8a), and the sum on $\vec{k}$ in Eq. (8b) runs through all the sites in the first Brillouin zone consistent with the Born-von Karman boundary condition.

Now, denoting the matrix element of the hamiltonian of a orbital μ in the unit cell at the origin and an orbital ν in the cell labeled by translation vector $\vec{T}''$,

$$H_{\mu\nu}(\vec{T}'') = \int_{\text{all space}}\mathrm{d}\vec{r}'\,\phi^*_\mu(\vec{r}'-\vec{\tau}_\mu)\hat{H}\phi_\nu(\vec{r}'-\vec{\tau}_\nu-\vec{T}''), \tag{9}$$

Eq. (7) transforms into

$$\langle\phi_\mu(\vec{k})|\hat{H}|\phi_\nu(\vec{k}')\rangle = N\delta_{\vec{k},\vec{k}'}A^*_{\mu\vec{k}}A_{\nu\vec{k}'}\left(\sum_{\vec{T}''}e^{i\vec{k}'\cdot\vec{T}''}H_{\mu,\nu}(\vec{T}'')\right). \tag{10}$$

Finally, assuming that the normalization factors of the Bloch orbitals are $\frac{1}{\sqrt{N}}$, we finally arrive to

$$H_{\mu\nu}(\vec{k}) = \langle\phi_\mu(\vec{k})|H|\phi_\nu(\vec{k})\rangle = \sum_{\vec{T}}e^{i\vec{k}\cdot\vec{T}}H_{\mu\nu}(\vec{T}). \tag{11}$$

2.1.3 The Overlap matrix elements

By analogy, the matrix elements of the overlap matrix between Bloch basis orbitals $\phi_\mu(\vec{k})$ and $\phi_\nu(\vec{k}')$ are also diagonal in $\vec{k}$ and equals

$$S_{\mu\nu}(\vec{k}) = \langle\phi_\mu(\vec{k})|\phi_\nu(\vec{k})\rangle = \sum_{\vec{T}}e^{i\vec{k}\cdot\vec{T}}S_{\mu\nu}(\vec{T}). \tag{12}$$

2.1.4 The secular equation

Since the hamiltonian conserves $\vec{k}$, an eigenfunction of the Schrödinger equation, $\psi_{n\vec{k}}(\vec{r})$, can be approximated as a linear combination of atomic orbitals, that can be written in the form

$$\psi_{n\vec{k}}(\vec{r}) = \sum_{\mu} c_{\mu n}(\vec{k})\phi_{\mu\vec{k}}(\vec{r}). \tag{13}$$

Inserting this expansion of the eigenfunctions into the Schrödinger equation,

$$\begin{aligned} &\hat{H}\psi_{n\vec{k}}(\vec{r}) = \varepsilon_n(\vec{k})\psi_{n\vec{k}}(\vec{r}), \\ &\hat{H}\left(\sum_{\mu} c_{\mu n}(\vec{k})\phi_{\mu\vec{k}}(\vec{r})\right) = \sum_{\mu} c_{\mu n}(\vec{k})\hat{H}\phi_{\mu\vec{k}}(\vec{r}) = \varepsilon_n(\vec{k})\sum_{\mu} c_{\mu n}(\vec{k})\phi_{\mu\vec{k}}(\vec{r}), \end{aligned} \tag{14}$$

Multiplying both sides of Eq. (14) by $\phi^*_{\nu\vec{k}}(\vec{r})$ and integrating over all space,

$$\begin{aligned} &\sum_{\mu} c_{\mu n}(\vec{k}) \int_{\text{all space}} \mathrm{d}\vec{r}\phi^*_{\nu\vec{k}}(\vec{r})\hat{H}\phi_{\mu\vec{k}}(\vec{r}) = \varepsilon_n(\vec{k})\sum_{\mu} c_{\mu n}(\vec{k}) \int_{\text{all space}} \mathrm{d}\vec{r}\phi^*_{\nu\vec{k}}(\vec{r})\phi_{\mu\vec{k}}(\vec{r}), \\ &\sum_{\mu} c_{\mu n}(\vec{k})H_{\nu\mu}(\vec{k}) = \varepsilon_n(\vec{k})\sum_{\mu} c_{\mu n}(\vec{k})S_{\nu\mu}(\vec{k}). \end{aligned} \tag{15}$$

Transposing all the terms to the left hand side in Eq. (15),

$$\sum_{\mu}\left(H_{\nu\mu}(\vec{k}) - \varepsilon_n(\vec{k})S_{\nu\mu}(\vec{k})\right)c_{\mu n}(\vec{k}) = 0. \tag{16}$$

This secular equation can be written in matrix notation as

$$\begin{pmatrix} \\ H(\vec{k}) \\ \\ \end{pmatrix}_{N\times N}\begin{pmatrix} c_n(\vec{k}) \\ \\ \end{pmatrix}_{N\times 1} = \varepsilon_n(\vec{k})\begin{pmatrix} \\ S(\vec{k}) \\ \\ \end{pmatrix}_{N\times N}\begin{pmatrix} c_n(\vec{k}) \\ \\ \end{pmatrix}_{N\times 1} \tag{17}$$

Non-trivial solutions (matrix of coefficients different from zero) can be found solving the secular equation, which is immediately obtained from Eq. (16),

$$|H(\vec{k}) - \varepsilon_n(\vec{k})S(\vec{k})| = 0. \tag{18}$$

2.2 Tight-binding model for a one-dimensional monoatomic chain

2.2.1 No dimerization case: one atom per unit cell

We can particularize the previous formalism to the case of a one-dimensional monoatomic solid consisting of Hydrogen atoms with lattice parameter a, as shown in Fig. 1.

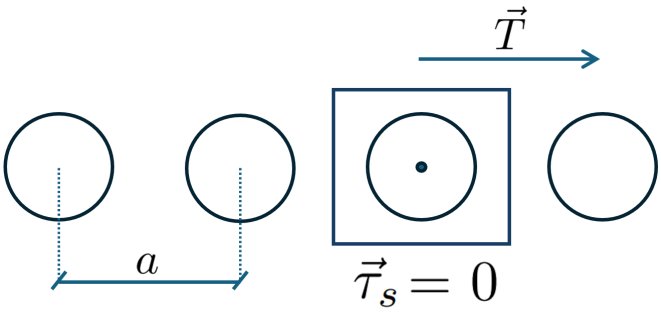

Figure 1: Sketch of a linear chain with one atom per unit cell, separated by a lattice constant a.

Let us assume the most simple case, where each atom contributes with only one orbital of s-symmetry, $\phi_s(\vec{r}-\vec{\tau}_s-\vec{T})$, where $\vec{\tau}_s$ is the position within the unit cell, and $\vec{T}$ is a translation vector of the Bravais lattice. From now on, and since we shall work in the one-dimensional system, the vector symbols will be omitted. Also, the electron will be considered spinless, in order to ignore magnetic interactions.

We can consider the unit cell made of only one atom. In such a case, the number of orbitals in the unit cell amounts to $N = 1$, and the Hamiltonian [Eq. (11)] and Overlap [Eq. (12)] matrices in k-space are just complex numbers.

Besides, we shall apply the following approximations to make the problem tractable from an analytical point of view:

- Localised orbitals: considering that the radial parts of the atomic orbitals decay rapidly in relatively small distances, the matrix elements of the Hamiltonian in real space, $H_{\nu\mu}(T)$ [Eq. (9)], will be neglected for translations vectors of the Bravais lattice whose magnitude is greater than the lattice parameter. In other words, $H_{\nu\mu}(T) = 0$ if $|T| > a$. That is, we shall consider on-site ($T = 0$) and first-neighbours ($T = \pm a$) interactions. These last hopping terms [$H_{\mu\nu}(T = \pm a) = \gamma$] will determine the width of the band. In this work, we shall consider $\gamma < 0$.
- The on-site energy of an orbital, $H_{\mu\mu}(T = 0) = \alpha$, determines the center of the band. Therefore, the origin of the potential energies is always ill-defined. We can set $\alpha = 0$ without loss of generality.
- Lastly, the orbitals are considered to be orthogonal, that is, they overlap only with themselves, such that $S_{\nu\mu} = 1 \iff \mu = \nu,\ T = 0$, and zero otherwise.

Once the approximations have been set, one can proceed and determine the hamiltonian and overlap matrix elements for a given value of k within the first Brillouin-zone. According to Eq. (11),

$$\begin{aligned} H_{\mu\nu}(k) &= \sum_T e^{ikT} H_{\mu\nu}(T) \\ &= e^{ik0} H_{\mu\mu}(T = 0) + e^{ika} H_{\mu\mu}(T = a) + e^{-ika} H_{\mu\mu}(T = -a) \\ &= \alpha + \gamma \left(e^{ika} + e^{-ika}\right) \\ &= \alpha + 2\gamma \cos(ka). \end{aligned} \tag{19}$$

A similar argument for the Overlap matrix elements in reciprocal space [Eq. (12)]

$$\begin{aligned} S_{\mu\nu}(k) &= \sum_T e^{ikT} S_{\mu\nu}(T) \\ &= e^{ik0} S_{\mu\mu}(T = 0) \\ &= 1. \end{aligned} \tag{20}$$

Therefore, the secular equation [Eq. (18)] is reduced to

$$\alpha + 2\gamma \cos(ka) - \varepsilon(k) = 0, \tag{21}$$

and solving for the eigenvalues $\varepsilon(k)$,

$$\varepsilon(k) = \alpha + 2\gamma \cos(ka) \tag{22}$$

$$= 2\gamma \cos(ka), \tag{23}$$

where we have assumed that $\alpha = 0$. Figure 2 represents the band structure for our simplified model.

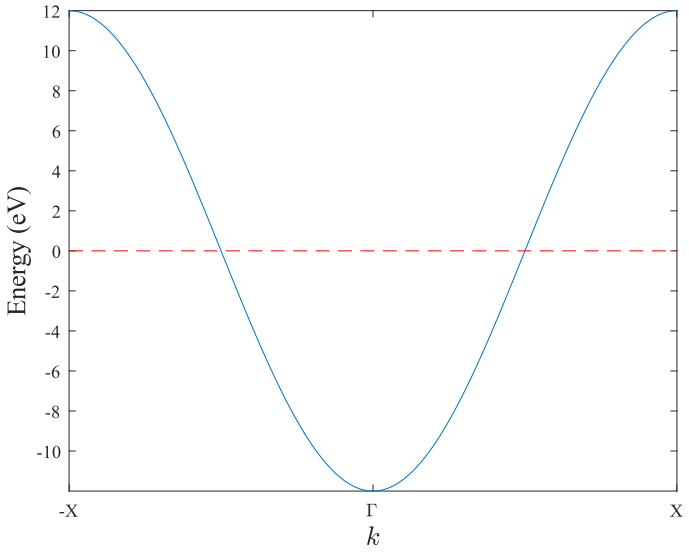

Figure 2: Graphical representation of the electronic energy band for a linear Hydrogen chain with one s-symmetry orbital per unit cell. We have taken a hopping of $\gamma = -6$ eV and the origin of energies exactly at the orbital on-site energy, α. The red dashed line represents the Fermi level.

Since each hydrogen contributes with one electron to the system, at absolute zero all energy levels up to the Fermi level, for which $k = k_{\mathrm{F}}$, are occupied, so the band is exactly half-filled, and therefore $k_{\mathrm{F}} = \pi/2a$. It can be seen that the electronic band in this simple model displays a cosine shape, with a total width of 4γ. It has maxima at the edges of the first Brillouin zone (1BZ) ($k = \pi/a \equiv$ X), and a minimum in its center ($k = 0 \equiv \Gamma$). The minimum is due to the fact that the phases of the electron wave functions are such that the system is in a maximally bonding state, while the maxima corresponds to a state in which the phases are alternating, and therefore maximally anti-bonding, as sketched in Fig. 3.

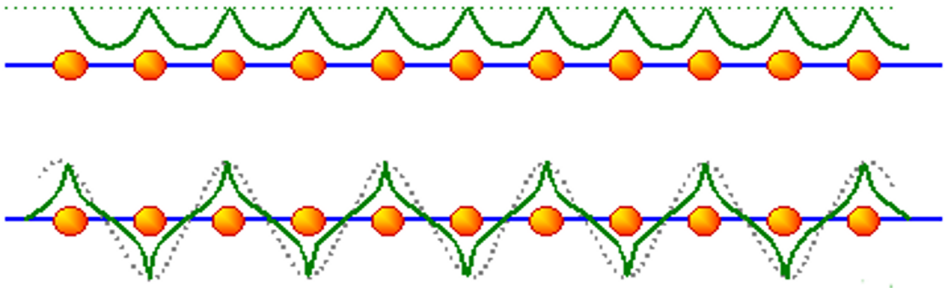

Figure 3: Maximally bonding (up) and antibonding (down) configurations. The green line represents the amplitude of the wavefunction of the electrons of the solid.

As it can be seen, the Fermi level crosses the electronic band, and there is no gap that separates the valence and conduction bands. This implies that the electrons can easily move through the different energy levels. This simplified model is a typical band metal.

Ground-state electronic energy per unit length

The ground-state electronic energy per unit length is crucial in later discussions on the stability of the solid. To compute the band-structure electronic energy, we sum the eigenvalues of the Hamiltonian over all the occupied states,

$$E_{\mathrm{elec}} = 2\sum_{n,k} f(\varepsilon, T)\varepsilon_n(k), \tag{24}$$

where the factor of 2 is due to the spin degeneracy, and $f(\varepsilon, T)$ is the occupation function given by the Fermi-Dirac distribution, which accounts for the Fermi-Dirac statistics at a given temperature T.

Assuming a one-dimensional system, the volume per k point in the reciprocal lattice is $\Delta k = \frac{2\pi}{L}$, where L is the length of the chain. Within the geometry of our one-dimensional model, L is an integer multiple, N, the number of atoms that compose the chain, of the lattice constant a,

$$L = Na. \tag{25}$$

Multiplying and dividing Eq. (24) by the volume per allowed k point,

$$\begin{aligned} E_{\text{elec}} &= 2\sum_{n,k} f(\varepsilon, T)\varepsilon_n(k)\frac{\Delta k}{\Delta k} \\ &= 2\sum_{n,k} f(\varepsilon, T)\varepsilon_n(k)\frac{\Delta k}{2\pi}L, \end{aligned} \tag{26}$$

dividing by L the two terms of the previous equation,

$$\frac{E_{\text{elec}}}{L} = \frac{1}{\pi}\sum_{n,k} f(\varepsilon, T)\varepsilon_n(k)\Delta k. \tag{27}$$

Since in this case the electronic energy is a quantity that varies smoothly over distances in the reciprocal space [19], one can comfortably assume the thermodynamic limit, i.e. $L \to \infty$. Under this condition, the distance between allowed k points tends to zero ($\Delta k \to 0$), and the sums over k points can be replaced by an integral. Thus,

$$\lim_{L\to\infty} \frac{E_{\text{elec}}}{L} = \frac{1}{\pi}\int_{1\text{BZ}} f(\varepsilon, T)\varepsilon_n(k)\mathrm{d}k, \tag{28}$$

where the integral is taken over the first Brillouin-zone.

For $T = 0$, which is the case since we are studying the ground-state electronic energy, the Fermi-Dirac distribution reduces to

$$f(\varepsilon, T = 0) = \begin{cases} 1 & \text{if } k \leq |k_{\text{F}}| = \frac{\pi}{2a} \\ 0 & \text{otherwise} \end{cases} \tag{29}$$

Replacing in Eq. (28) the functional form for the dispersion relation of the eigenvalues as a function of k [Eq. (23)], and the Fermi-Dirac distribution for $T = 0$ [Eq. (29)],

$$\begin{aligned} \lim_{L\to\infty} \frac{E_{\text{elec}}}{L} &= \frac{1}{\pi}\int_{-\pi/a}^{\pi/a} f(\varepsilon, T = 0)\cdot 2\gamma\cos(ka)\mathrm{d}k \\ &= \frac{1}{\pi}\int_{-\pi/2a}^{\pi/2a} 2\gamma\cos(ka)\mathrm{d}k \\ &= \frac{2}{\pi}\int_{0}^{\pi/2a} 2\gamma\cos(ka)\mathrm{d}k \\ &= \frac{4\gamma}{\pi a}\int_{0}^{\pi/2a} a\cos(ka)\mathrm{d}k \\ &= \frac{4\gamma}{\pi a}\sin(ka)\Big|_{k=0}^{k=\pi/2a} \\ &= \frac{4\gamma}{\pi a}\sin\left(\frac{\pi}{2}\right) \\ &= \frac{4\gamma}{\pi a}, \end{aligned} \tag{30}$$

which is the ground-state electronic energy per unit length of the monoatomic hydrogen chain.

Density of states with one atom per unit cell

In a solid, the density of states (DOS) in the n-th band, $g_n(\varepsilon)$, can be defined as the number of allowed wave-vectors in that band with energies within the range $(\varepsilon, \varepsilon + \mathrm{d}\varepsilon)$, divided by the volume of the system in real space, V. The number of allowed wave-vectors is just the volume of the $\vec{k}$-space in the 1^{st} Brillouin Zone with $\varepsilon \leq \varepsilon_n(\vec{k}) \leq \varepsilon + \mathrm{d}\varepsilon$, divided by the volume per allowed $\vec{k}$-vector, $\Delta\vec{k} = \frac{(2\pi)^3}{V}$.

This volume can be computed as a surface integral in the reciprocal space [See Ref. [19], Chapter 8],

$$g_n(\varepsilon)\mathrm{d}\varepsilon = 2\int_{S_n(\varepsilon)} \frac{\mathrm{d}S}{\frac{(2\pi)^3}{V}} \delta k(\vec{k}), \tag{31}$$

where $S_n(\varepsilon)$ is a portion of the surface with $\varepsilon_n(\vec{k}) = \varepsilon$, and $\delta k(\vec{k})$ is the perpendicular distance between the surfaces $S_n(\varepsilon)$ and $S_n(\varepsilon + \mathrm{d}\varepsilon)$ at $\vec{k}$. The factor of 2 is due to the spin degeneracy.

In order to find an explicit expression for $\delta k(\vec{k})$, note that $S_n(\varepsilon)$ is a constant energy surface. Therefore, the k-gradient of $\varepsilon_n(\vec{k})$, $\nabla\varepsilon_n(\vec{k})$, is a vector normal to the surface with modulus equal to the rate of change of $\varepsilon_n(\vec{k})$ in the normal direction, thus,

$$\varepsilon + \mathrm{d}\varepsilon = \varepsilon + |\nabla\varepsilon_n(\vec{k})|\delta k(\vec{k}) \implies \delta k(\vec{k}) = \frac{\mathrm{d}\varepsilon}{|\nabla\varepsilon_n(\vec{k})|}. \tag{32}$$

Replacing this in Eq. (31),

$$g_n(\varepsilon) = 2\int_{S_n(\varepsilon)} \frac{V}{(2\pi)^3} \frac{\mathrm{d}S}{|\nabla\varepsilon_n(\vec{k})|}. \tag{33}$$

Let us particularize to the case of the monoatomic chain:

- One-dimensional: $\vec{k} \to k$. Besides, the volume per allowed k-point takes the value $\Delta k = \frac{2\pi}{L}$.
- One atom per unit cell: there is just one band, therefore, we can omit the band index n.
- Analytic expression for the eigenvalues of the Hamiltonian operator [Eq. (22)],

$$\varepsilon(k) = \alpha + 2\gamma\cos(ka). \tag{34}$$

- The gradient can be determined analytically:

$$\nabla\varepsilon(k) = \frac{\mathrm{d}\varepsilon(k)}{\mathrm{d}k} = -2\gamma a\sin(ka). \tag{35}$$

- The surface in the reciprocal space is restricted to two points, those where the band intersect with the given energy plane, $\varepsilon(k) = \varepsilon$. Thus, we can write

$$\begin{aligned}\mathrm{d}S &= \delta\left[\varepsilon - \varepsilon(k)\right]\mathrm{d}k \\ &= \delta\left[\varepsilon - (\alpha + 2\gamma\cos(ka))\right]\mathrm{d}k.\end{aligned} \tag{36}$$

  where δ denotes the Dirac delta function. The k points that compose the surface, i.e. that verify $\delta\left[\varepsilon - \varepsilon(k)\right] \neq 0$, must accomplish the condition

$$\varepsilon = \alpha + 2\gamma\cos(ka), \tag{37}$$

  thus,

$$k = \pm\frac{1}{a}\arccos\left(\frac{\varepsilon - \alpha}{2\gamma}\right). \tag{38}$$

Introducing this considerations in Eq. (33),

$$
\begin{aligned}
g(\varepsilon) &= 2\int_{1\mathrm{BZ}} \frac{L\cdot\delta\left[\varepsilon-(\alpha+2\gamma\cos(ka))\right]}{2\pi|-2\gamma a\sin(ka)|}\mathrm{d}k \\
&= \frac{1}{2\pi a\left|\gamma\sin\left(\frac{L}{a}\arccos\left(\frac{\varepsilon-\alpha}{2\gamma}\right)\cdot a\right)\right|} + \frac{L}{2\pi a\left|\gamma\sin\left(-\frac{1}{a}\arccos\left(\frac{\varepsilon-\alpha}{2\gamma}\right)\cdot a\right)\right|} \\
&= \frac{L}{\pi a\left|\gamma\sin\left(\arccos\left(\frac{\varepsilon-\alpha}{2\gamma}\right)\right)\right|} \\
&= \frac{L}{\pi a\left|\gamma\sqrt{1-\frac{(\varepsilon-\alpha)^2}{4\gamma^2}}\right|} \\
&= \frac{2L}{\pi a\sqrt{4\gamma^2-(\varepsilon-\alpha)^2}} \\
&= \frac{2N}{\pi\sqrt{4\gamma^2-(\varepsilon-\alpha)^2}},
\end{aligned}
\tag{39}
$$

that is, the density of states the one-dimensional monoatomic chain. It has been taken into account that $|\sin(x)| = |\sin(-x)|$, the relation $\sin(\arccos(x)) = \sqrt{1-x^2}$ and the fact that $L = Na$. The density of states is defined in the range

$$-2|\gamma| \leq \varepsilon - \alpha \leq 2|\gamma|, \tag{40}$$

the band width, where the argument of the square root is positive and the bands are defined. Figure 4 shows the relation between the density of states and the energy.

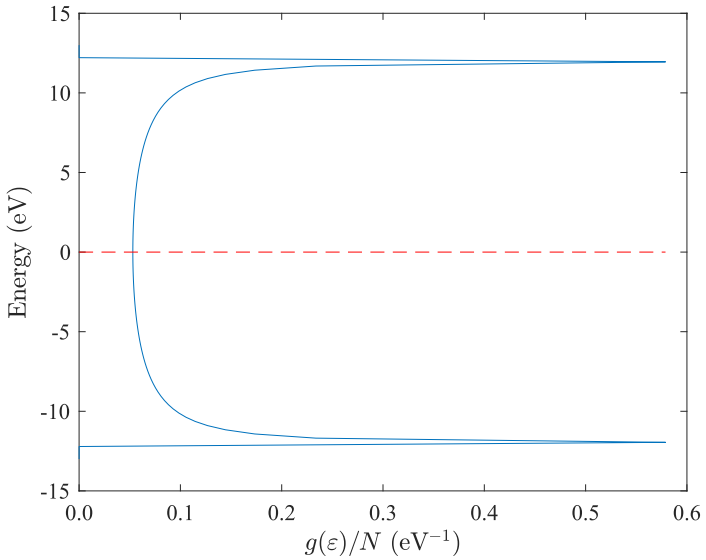

Figure 4: Graphical representation of the density of states of the one-dimensional monoatomic Hydrogen chain with one s-symmetry orbital per unit cell. We have taken a hopping of $\gamma = -6$ eV and the origin of energies exactly at the orbital on-site energy, α. The red dashed line represents the Fermi level.

In Fig. 4 it can be seen that the density of states reaches its highest values at the Γ point and at the zone edge, $k = \pm$ X, where the electronic bands exhibit flatter regions. The DOS is at its minimum at the Fermi level, $k = k_{\mathrm{F}}$, where the band gradient is the largest. Near the Fermi level, it remains relatively constant, indicating that most of the states are concentrated around the Γ and $\pm$ X points.

2.2.2 No dimerization case: two atoms per unit cell

In this section, we will particularize the tight-binding formalism to the monoatomic chain considering two atoms per unit cell, each one contributing with one orbital of s-symmetry, $\phi_s(r-\tau_s-T)$, as shown in Fig. 5.

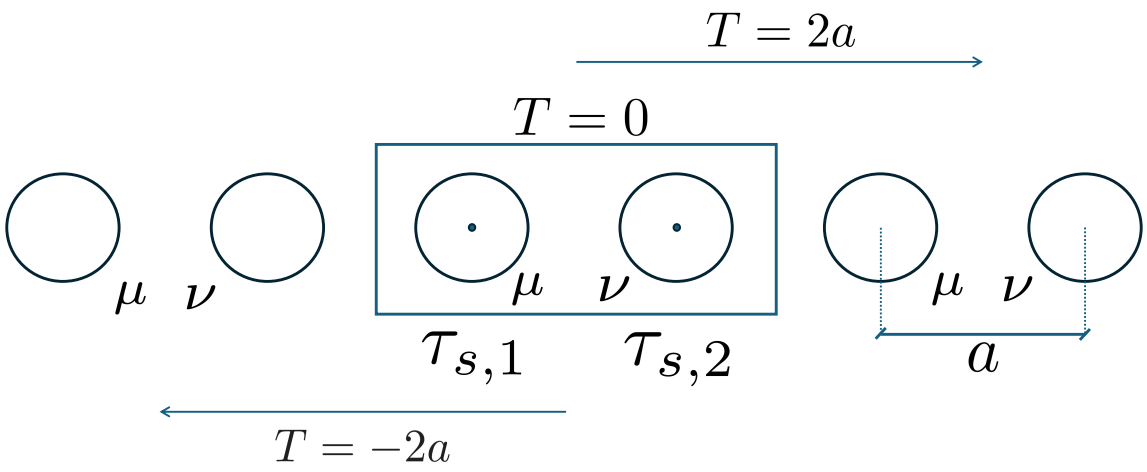

Figure 5: Sketch of a linear chain with two atoms per unit cell.

The number of orbitals in the unit cell is $N = 2$, and the Hamiltonian [Eq. (11)] and Overlap [Eq. (12)] operators in k-space are (2×2) complex matrices.

We shall follow the same approximations and assumptions considered previously in Sec 2.2.1, particularized for this configuration:

- Localised orbitals: The matrix elements of the Hamiltonian in real space, $H_{\nu\mu}(T)$ [Eq. (9)], will be neglected for orbitals separated by a distance larger than the interatomic distance. Therefore, $H_{\mu\mu}(|T| \geq 2a) = H_{\nu\nu}(|T| \geq 2a) = 0$. That is, we shall consider on-site and first-neighbour interactions. The hopping terms,

$$\begin{aligned} H_{\mu\nu}(T = 0) &= H_{\mu\nu}(T = -2a) = \gamma, \\ H_{\nu\mu}(T = 0) &= H_{\nu\mu}(T = +2a) = \gamma, \end{aligned} \tag{41}$$

  with $\gamma < 0$, will determine the width of the band.

- The on-site energy of the orbitals, $H_{\mu\mu}(T = 0) = H_{\nu\nu}(T = 0) = \alpha$, determines the center of the band. We can set $\alpha = 0$ without loss of generality.

- The orbitals are considered to be orthogonal, such that $S_{\mu\nu} = 1 \iff \mu = \nu, T = 0$, and zero otherwise.

For the Hamiltonian, the elements of the matrix can be computed using Eq. (11):

$$\begin{aligned} H_{11}(k) &= \sum_T e^{ikT} H_{11}(T) = e^{ik0} H_{11}(T = 0) = \alpha, \\ H_{12}(k) &= \sum_T e^{ikT} H_{12}(T) = e^{ik0} H_{12}(T = 0) + e^{-ik2a} H_{12}(T = -2a) = \gamma \left(1 + e^{-ik2a}\right), \\ H_{21}(k) &= \sum_T e^{ikT} H_{21}(T) = e^{ik0} H_{21}(T = 0) + e^{ik2a} H_{21}(T = 2a) = \gamma \left(1 + e^{ik2a}\right), \\ H_{22}(T) &= \sum_T e^{ikT} H_{22}(T) = e^{ik0} H_{22}(T = 0) = \alpha. \end{aligned} \tag{42}$$

For the overlap matrix, we apply Eq. (12),

$$\begin{aligned} S_{11}(T) &= \sum_T e^{ikT} S_{11}(T) = e^{ik0} S_{11}(T = 0) = 1, \\ S_{12}(T) &= \sum_T e^{ikT} S_{12}(T) = 0, \\ S_{21}(T) &= \sum_T e^{ikT} S_{21}(T) = 0, \\ S_{22}(T) &= \sum_T e^{ikT} S_{22}(T) = e^{ik0} S_{22}(T = 0) = 1. \end{aligned} \tag{43}$$

Replacing these matrix elements in the secular equation [Eq. (18)],

$$\begin{vmatrix} \alpha - \varepsilon_n(k) & \gamma\left(1 + e^{-ik2a}\right) \\ \gamma\left(1 + e^{ik2a}\right) & \alpha - \varepsilon_n(k) \end{vmatrix} = 0. \tag{44}$$

Therefore,

$$\begin{aligned} 0 &= \left(\alpha - \varepsilon_n(k)\right)^2 - \gamma^2\left(1 + e^{ik2a}\right)\left(1 + e^{-ik2a}\right) \\ &= \alpha^2 + \varepsilon_n^2(k) - 2\alpha\varepsilon_n(k) - \gamma^2\left(2 + e^{ik2a} + e^{-ik2a}\right) \\ &= \varepsilon_n^2(k) - 2\alpha\varepsilon_n(k) + \alpha^2 - 2\gamma^2\left(1 + \cos(k2a)\right). \end{aligned} \tag{45}$$

Solving for $\varepsilon_n(k)$,

$$\begin{aligned} \varepsilon_n(k) &= \alpha \pm 2\gamma\cos(ka) \\ &= \pm 2\gamma\cos(ka), \end{aligned} \tag{46}$$

one obtains the expression for the eigenvalues of the Hamiltonian operator, where we have assumed that $\alpha = 0$. Figure 6 represents the band structure in this simplified model.

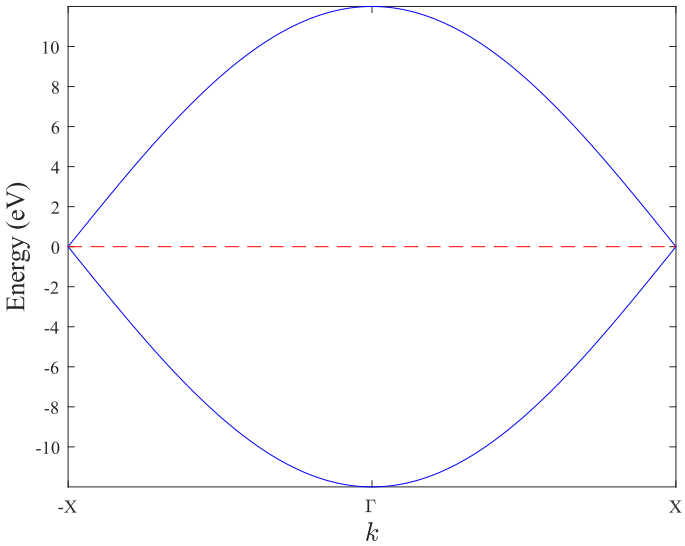

Figure 6: Graphical representation of the electronic energy band for a linear Hydrogen chain with two atoms and two s-symmetry orbitals per unit cell. We have taken a hopping of $\gamma = -6$ eV and the origin of energies exactly at the orbital on-site energy, α. The red dashed line represents the Fermi level.

It can be seen that the electronic bands are essentially the same as in the case of one atom per unit cell, Fig. 2, but reducing the length of the first Brillouin zone by half, thus causing the band to fold at the Fermi level, resulting in two branches which are not separated by an energy gap. Therefore, there is a degeneracy at the Fermi level, $k = k_{\mathrm{F}}$.

Ground-state electronic energy per unit length

The ground-state electronic energy per unit length of the system is exactly the same as the one obtained in Sec. 2.2.1, since the only difference with respect to the previous case is the definition of the unit cell.

Density of states with two atoms per unit cell

The density of states per unit length of the system remains qualitatively the same as the one obtained for the one atom per unit cell case [Sec. 2.2.1]. The only difference is that the lattice parameter has been doubled, therefore, the length of the 1^{st} Brillouin Zone has been reduced by half and there are two electronic bands

instead of one. Consequently, there are two densities of states, one per band, with $n = 1$ (lower band) and $n = 2$ (upper band), which are exactly the same since the bands are symmetric:

$$g_{n=1,2(\varepsilon)} = \frac{N}{\pi\sqrt{4\gamma^2 - (\varepsilon - \alpha)^2}}. \tag{47}$$

2.2.3 Dimerized case (two atoms per unit cell)

When the linear chain dimerizes, the distance between consecutive Hydrogen atoms changes, alternating short and long-distance bonds. As a consequence, the hopping parameters characterizing the strong (short-distance) and weak (long-distance) bonds are different. Within this model, there are two tight-binding sites per unit cell, having alternating hopping parameters $\gamma - \delta$ and $\gamma + \delta$, respectively. Since, as we have already mentioned before, we are taking the hopping parameter $\gamma < 0$, and assuming that $\delta > 0$, then the hopping corresponding to $\gamma - \delta$ will be more negative and therefore reflects an stronger bonding between consecutive atoms. In the opposite way, $\gamma + \delta$ will be less negative and points to a weaker interatomic bonding. This configuration is shown in Fig. 7.

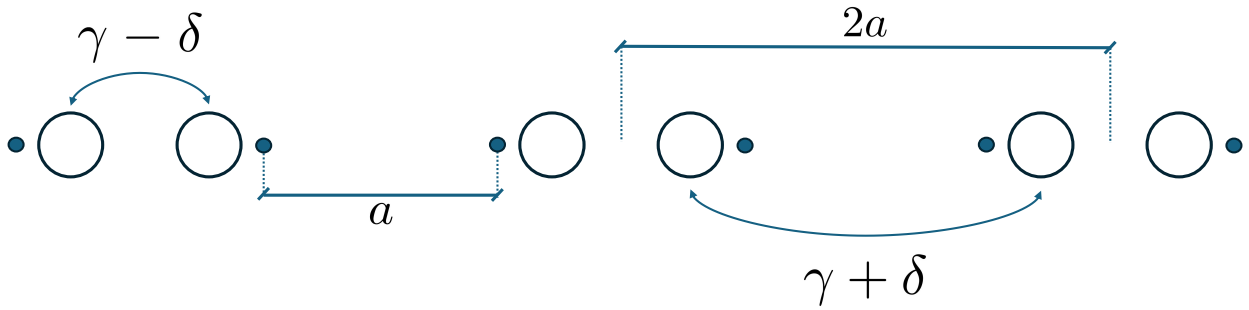

Figure 7: Sketch of a dimerized linear chain with different hopping parameters for long and short bonds.

In order to determine the Hamiltonian and Overlap matrices, we shall proceed in the same manner as in Sec. 2.2.2.

Regarding the Hamiltonian matrix elements [Eq. (11)],

$$\begin{aligned}
H_{11}(k) &= \sum_T e^{ikT} H_{11}(T) = e^{ik0} H_{11}(T=0) = \alpha, \\
H_{12}(k) &= \sum_T e^{ikT} H_{12}(T) = e^{ik0} H_{12}(T=0) + e^{-ik2a} H_{12}(T=-2a) = (\gamma - \delta) + e^{-ik2a}(\gamma + \delta), \\
H_{21}(k) &= \sum_T e^{ikT} H_{21}(T) = e^{ik0} H_{21}(T=0) + e^{ik2a} H_{21}(T=2a) = (\gamma - \delta) + e^{ik2a}(\gamma + \delta), \\
H_{22}(k) &= \sum_T e^{ikT} H_{22}(T) = e^{ik0} H_{22}(T=0) = \alpha.
\end{aligned} \tag{48}$$

On the other hand, for the overlap matrix [Eq. (12)],

$$\begin{aligned}
S_{11}(k) &= \sum_T e^{ikT} S_{11}(T) = S_{11}(T=0) = 1, \\
S_{12}(k) &= \sum_T e^{ikT} S_{12}(T) = 0, \\
S_{21}(k) &= \sum_T e^{ikT} S_{21}(T) = 0, \\
S_{22}(k) &= \sum_T e^{ikT} S_{22}(T) = S_{22}(T=0) = 1.
\end{aligned} \tag{49}$$

Replacing these matrix elements in the secular equation, Eq. (18) and considering again for the sake of simplicity that $\alpha = 0$,

$$\begin{vmatrix} -\varepsilon_n(k) & (\gamma - \delta) + (\gamma + \delta)e^{-ik2a} \\ (\gamma - \delta) + (\gamma + \delta)e^{ik2a} & -\varepsilon_n(k) \end{vmatrix} = 0. \tag{50}$$

Solving for $\varepsilon_n(k)$,

$$\begin{aligned}
\varepsilon_n^2(k) &= \left[(\gamma-\delta)+(\gamma+\delta)e^{-ik2a}\right]\left[(\gamma-\delta)+(\gamma+\delta)e^{ik2a}\right] \\
&= (\gamma-\delta)^2+(\gamma-\delta)(\gamma+\delta)\left(e^{ik2a}+e^{-ik2a}\right)+(\gamma+\delta)^2 \\
&= (\gamma-\delta)^2+(\gamma+\delta)^2+2(\gamma-\delta)(\gamma+\delta)\cos(2ka) \\
&= (\gamma-\delta)^2+(\gamma+\delta)^2+2(\gamma-\delta)(\gamma+\delta)(2\cos^2(ka)-1) \\
&= (\gamma-\delta)^2+(\gamma+\delta)^2-2(\gamma-\delta)(\gamma+\delta)+4(\gamma^2-\delta^2)\cos^2(ka) \\
&= ((\gamma-\delta)-(\gamma+\delta))^2+4(\gamma^2-\delta^2)\cos^2(ka) \\
&= 4\delta^2+4(\gamma^2-\delta^2)\cos^2(ka) \\
&= 4[\delta^2+(\gamma^2-\delta^2)\cos^2(ka)] \\
&= 4[\delta^2+\gamma^2\cos^2(ka)-\delta^2\cos^2(ka)] \\
&= 4[\delta^2(1-\cos^2(ka))+\gamma^2\cos^2(ka)] \\
&= 4[\gamma^2\cos^2(ka)+\delta^2\sin^2(ka)],
\end{aligned}$$

one obtains the expression for the eigenvalues of the Hamiltonian operator,

$$\varepsilon_n(k) = \pm 2\sqrt{\gamma^2\cos^2(ka)+\delta^2\sin^2(ka)}, \tag{51}$$

which can also be expressed as

$$\varepsilon_n(k) = \pm 2\sqrt{\delta^2+(\gamma^2-\delta^2)\cos^2(ka)}. \tag{52}$$

Notice that, if $\delta = 0$, one simply recovers the dispersion relation for the non-dimerized case, but considering two atoms per unit cell [Eq. (46)]. If $\alpha \neq 0$, the bands will remain exactly the same, but shifted vertically by an amount α,

$$\varepsilon_n(k) = \alpha \pm 2\sqrt{\gamma^2\cos^2(ka)+\delta^2\sin^2(ka)} \tag{53}$$

$$= \alpha \pm 2\sqrt{\delta^2+(\gamma^2-\delta^2)\cos^2(ka)}. \tag{54}$$

The graphical representation of the electronic bands of the dimerized and non-dimerized chains is shown in Fig. 8.

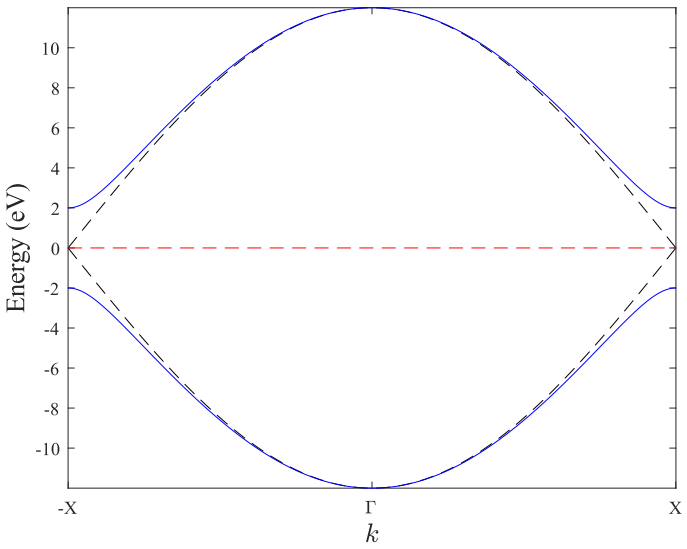

Figure 8: Electronic bands for the dimerized chain, according to Eq. (51), with parameters $\gamma = -6$ eV and $\delta = 1$ eV. The electronic bands for the non-dimerized case with two atoms per the unit cell (black dashed line) have been determined using Eq. (46). The X point is taken as the edge of the first Brillouin zone, considering two atoms in the unit cell in real space, X = $\pi/2a$. The red dashed line represents the Fermi level.

The dimerization of the system leads to the opening of a gap at the zone edge $\left(k = \frac{\pi}{2a}\right)$, whose amplitude according to Eq. (51) amounts to

$$E_{\text{gap}} = 4|\delta|. \tag{55}$$

The equidistant configuration of the system results in degeneracy at the Fermi level. However, dimerization lifts this degeneracy, creating a gap at the zone edge that separates the valence and conduction bands. Electrons with wave-vector k near the Fermi surface have their energy lowered due to this lattice deformation. This behavior indicates that the dimerized system has a lower electronic energy, since the electrons at the valence band near k_{F} have lower energies.

The opening of a gap at the zone edge results in a metal-insulator transition. The electronic characteristics of the dimerized system will be determined by δ. Although our calculations assume $T = 0$, we can ascertain the behaviour of the system at finite temperature for different values of δ. If δ is large, the gap amplitude will be such that very few electrons reach the conduction band due to thermal excitations, resulting in low electronic conductivity. Conversely, for small values of δ, the dimerized system can be considered an intrinsic semiconductor.

Variation in electronic energy per unit length of the dimerized chain

As will be shown in Sec. 2.3.2, the dimerization of the system leads to an increase in the elastic energy of the chain. To determine whether the Peierls transition takes place spontaneously, it is necessary to compute the variation in the electrostatic energy of the solid per unit length when the system dimerizes and a band gap is opened, as shown in Fig. 8. This quantity shall be calculated in the thermodynamic limit, where it takes the form

$$\lim_{L\to\infty} \frac{\Delta E_{\text{elec}}}{L} = \frac{1}{\pi} \int_{-\pi/2a}^{\pi/2a} \left[\varepsilon_{\text{elec}}^{\text{dim}}(k) - \varepsilon_{\text{elec}}^{\text{non dim}}(k)\right] \mathrm{d}k, \tag{56}$$

where $\varepsilon_{\text{elec}}^{\text{dim}}(k)$ are the eigenvalues when the system is dimerized [Eq. (51)], and $\varepsilon_{\text{elec}}^{\text{non dim}}(k)$ are the eigenvalues in the absence of dimerization [Eq. (46)]. Given that we are interested in the energy gain, only the occupied bands (lower ones in Fig. 8) are taken into account. Since we are considering that $\gamma < 0$, we have to take the solution with the minus sign in Eq. (51), and the plus sign in Eq. (46). Replacing this dispersion relations in Eq. (56)

$$\begin{aligned}\lim_{L\to\infty} \frac{\Delta E_{\text{elec}}}{L} &= \frac{1}{\pi} \int_{-\pi/2a}^{\pi/2a} \left[-2\sqrt{\gamma^2\cos^2(ka) + \delta^2\sin^2(ka)} - 2\gamma\cos(ka)\right] \mathrm{d}k \\ &= \frac{2}{\pi} \int_{0}^{\pi/2a} \left[-2\sqrt{\gamma^2\cos^2(ka) + \delta^2\sin^2(ka)} - 2\gamma\cos(ka)\right] \mathrm{d}k.\end{aligned} \tag{57}$$

Introducing the following change of variables: $\theta = ka$, and noting that $-\gamma = |\gamma|$,

$$\lim_{L\to\infty} \frac{\Delta E_{\text{elec}}}{L} = \frac{2}{\pi a} \int_{0}^{\pi/2} \left[-2|\gamma|\sqrt{\cos^2(\theta) + \frac{\delta^2}{\gamma^2}\sin^2(\theta)} + 2|\gamma|\cos(\theta)\right] \mathrm{d}\theta. \tag{58}$$

Defining $\lambda \equiv \delta^2/\gamma^2$,

$$\begin{aligned}\lim_{L\to\infty} \frac{\Delta E_{\text{elec}}}{L} &= -\frac{4|\gamma|}{\pi a} \int_{0}^{\pi/2} \left[\sqrt{\cos^2(\theta) + \lambda\sin^2(\theta)} - \cos(\theta)\right] \mathrm{d}\theta \\ &= -\frac{4|\gamma|}{\pi a} \int_{0}^{\pi/2} \left[\sqrt{1 - \sin^2(\theta) + \lambda\sin^2(\theta)} - \cos(\theta)\right] \mathrm{d}\theta \\ &= -\frac{4|\gamma|}{\pi a} \int_{0}^{\pi/2} \left[\sqrt{1 - (1-\lambda)\sin^2(\theta)} - \cos(\theta)\right] \mathrm{d}\theta \\ &= -\frac{4|\gamma|}{\pi a} \left[\int_{0}^{\pi/2} \sqrt{1 - (1-\lambda)\sin^2(\theta)}\mathrm{d}\theta - 1\right].\end{aligned} \tag{59}$$

The integral $\int_0^{\pi/2}\sqrt{1-(1-\lambda)\sin^2(\theta)}\mathrm{d}\theta$ is a complete elliptic integral of the second kind, $E(1-\lambda)$. This kind of integral only has real solutions for $1-\lambda<1$ (see Appendix A), which is always true since $\lambda>0$ if the chain is dimerized. For values $\lambda<1$, it can be expanded as (See Appendix A and [20])

$$E\left(1-\lambda\right)=1+\lambda\left[0.443-\frac{1}{4}\ln(\lambda)\right]+\mathcal{O}(\lambda^2), \tag{60}$$

which is an useful result in order to approach this study with analytical expressions.

Therefore, the electrostatic energy variation per unit length between the dimerized and non-dimerized states can be approximated as

$$\begin{aligned}\lim_{L\to\infty}\frac{\Delta E_{\text{elec}}}{L}&\approx-\frac{4|\gamma|}{\pi a}\cdot\lambda\left[0.443-\frac{1}{4}\ln(\lambda)\right]\\&=\frac{4\gamma}{\pi a}\cdot\lambda\left[0.443-\frac{1}{4}\ln(\lambda)\right].\end{aligned} \tag{61}$$

Since $\lambda=\delta^2/\gamma^2>0$ and $\lambda<1$, then $\ln(\lambda)<0$. Therefore, the correction in the square brackets is positive. Thus, since $\gamma<0$, the electronic energy variation will always be negative. In other words, the system always gain electrostatic energy when it dimerizes.

The precision of this approximation [Eq. (61)] exhibits an strong dependency on λ. Figure 9 is a comparison between the values of the complete elliptic integral determined using MATLAB function *ellipticE* and the ones from the approximation above [Eq. (60)], as a function of λ. In Fig. 10 the relative error of the approximation is given as a function of λ.

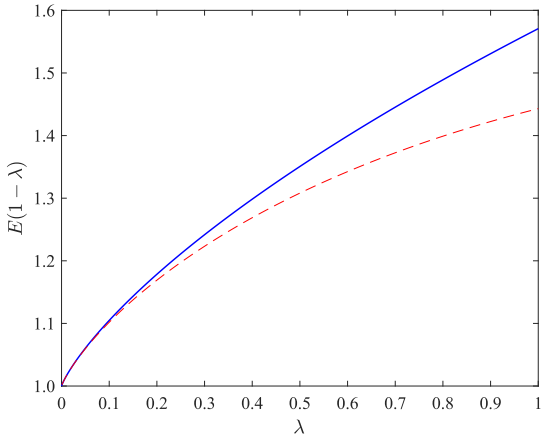

Figure 9: Value of the complete elliptic integral of the second kind as a function of λ, determined using the *ellipticE* function from MATLAB (blue line) and the approximation shown in Eq. (60) (red dashed line).

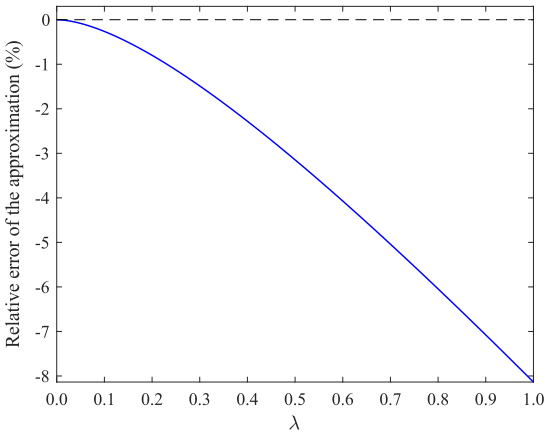

Figure 10: Relative error (%) of the approximation of the complete elliptic integral of the second kind [Eq. (60)].

Density of states of the dimerized chain

To determine the density of states of the dimerized chain, we shall proceed in the same manner as in the one atom per unit cell case, but particularizing for the dimerized system:

- Two atoms per unit cell: there are two electronic bands. The band index will take the value $n=1$ for the valence band and $n=2$ for the conduction band.
- The eigenvalues of the Hamiltonian operator [Eq. (54)],

$$\varepsilon_1(k)=\alpha-2\sqrt{\delta^2+(\gamma^2-\delta^2)\cos^2(ka)} \tag{62}$$

$$\varepsilon_2(k)=\alpha+2\sqrt{\delta^2+(\gamma^2-\delta^2)\cos^2(ka)} \tag{63}$$

- The k-gradient in energy:

$$\nabla\varepsilon_1(k) = +\frac{2a(\gamma^2-\delta^2)\sin(ka)\cos(ka)}{\sqrt{\delta^2+(\gamma^2-\delta^2)\cos^2(ka)}} \tag{64}$$

$$\nabla\varepsilon_2(k) = -\frac{2a(\gamma^2-\delta^2)\sin(ka)\cos(ka)}{\sqrt{\delta^2+(\gamma^2-\delta^2)\cos^2(ka)}} \tag{65}$$

- The k points that compose the constant energy surface accomplish the condition

$$\varepsilon = \alpha \pm 2\sqrt{\delta^2+(\gamma^2-\delta^2)\cos^2(ka)}. \tag{66}$$

  Since the bands are symmetric, the resulting k points will be the same for each band,

$$k = \pm\frac{1}{a}\arccos\left(\left[\frac{\left(\frac{\varepsilon-\alpha}{2}\right)^2-\delta^2}{\gamma^2-\delta^2}\right]^{\frac{1}{2}}\right). \tag{67}$$

Introducing this considerations in Eq. (33), we can determine the density of states of the dimerized chain for both bands, which is exactly the same since they are symmetric,

$$\begin{aligned}
g^{\dim}_{n=1,2}(\varepsilon) &= 2\int_{1\mathrm{BZ}} \frac{L\cdot\delta\left[\varepsilon-\left(\alpha\pm2\sqrt{\delta^2+(\gamma^2-\delta^2)\cos^2(ka)}\right)\right]}{2\pi\left|\pm\frac{2a(\gamma^2-\delta^2)\sin(ka)\cos(ka)}{\sqrt{\delta^2+(\gamma^2-\delta^2)\cos^2(ka)}}\right|}\mathrm{d}k \\
&= \frac{L\cdot\sqrt{\delta^2+(\gamma^2-\delta^2)\cos^2\left(\arccos\left(\left[\frac{\left(\frac{\varepsilon-\alpha}{2}\right)^2-\delta^2}{\gamma^2-\delta^2}\right]^{\frac{1}{2}}\right)\right)}}{2\pi a(\gamma^2-\delta^2)\sin\left(\arccos\left(\left[\frac{\left(\frac{\varepsilon-\alpha}{2}\right)^2-\delta^2}{\gamma^2-\delta^2}\right]^{\frac{1}{2}}\right)\right)\cos\left(\arccos\left(\left[\frac{\left(\frac{\varepsilon-\alpha}{2}\right)^2-\delta^2}{\gamma^2-\delta^2}\right]^{\frac{1}{2}}\right)\right)} \\
&= \frac{L\cdot\sqrt{\delta^2+(\gamma^2-\delta^2)\frac{\left(\frac{\varepsilon-\alpha}{2}\right)^2-\delta^2}{\gamma^2-\delta^2}}}{2\pi a(\gamma^2-\delta^2)\sqrt{1-\frac{\left(\frac{\varepsilon-\alpha}{2}\right)^2-\delta^2}{\gamma^2-\delta^2}}\sqrt{\frac{\left(\frac{\varepsilon-\alpha}{2}\right)^2-\delta^2}{\gamma^2-\delta^2}}} \\
&= \frac{L\cdot|\varepsilon-\alpha|}{4\pi a(\gamma^2-\delta^2)\sqrt{\frac{\gamma^2-\delta^2-\left(\frac{\varepsilon-\alpha}{2}\right)^2+\delta^2}{\gamma^2-\delta^2}}\sqrt{\frac{\left(\frac{\varepsilon-\alpha}{2}\right)^2-\delta^2}{\gamma^2-\delta^2}}} \\
&= \frac{L\cdot|\varepsilon-\alpha|}{4\pi a\sqrt{\gamma^2-\left(\frac{\varepsilon-\alpha}{2}\right)^2}\sqrt{\left(\frac{\varepsilon-\alpha}{2}\right)^2-\delta^2}} \\
&= \frac{N\cdot|\varepsilon-\alpha|}{\pi\sqrt{4\gamma^2-(\varepsilon-\alpha)^2}\sqrt{(\varepsilon-\alpha)^2-4\delta^2}}.
\end{aligned} \tag{68}$$

As it can be seen, by setting $\delta = 0$ one recovers the density of states of the no dimerization case with two atoms per unit cell [Eq. (47)]. In this case, the density of states is defined in the range

$$\varepsilon-\alpha \in [-2|\gamma|,\ -2\delta]\cup[2\delta,\ 2|\gamma|], \tag{69}$$

where the bands are defined and the arguments of the square roots are both positive. Figure 11 shows the relation between the density of states of the dimerized system and the energy.

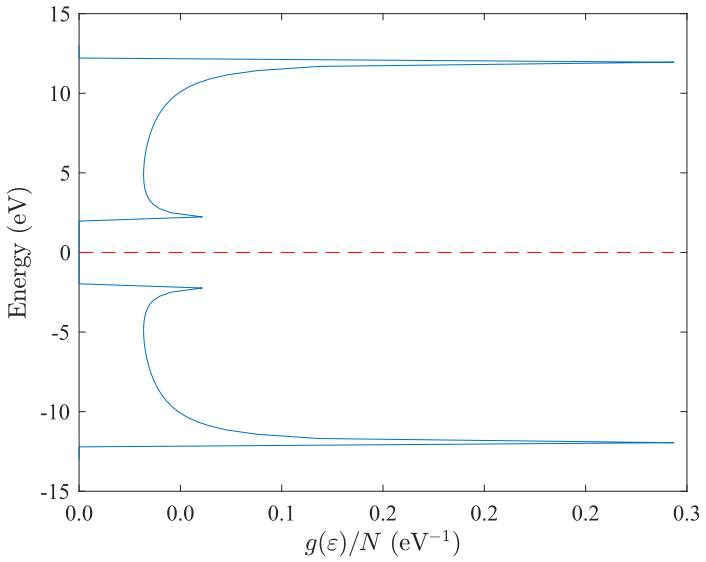

Figure 11: Graphical representation of the density of states of the dimerized one-dimensional monoatomic Hydrogen chain with two s-symmetry orbitals per unit cell. We have taken a hopping of $\gamma = -6$ eV, and a correction term of $\delta = 1$ eV. The origin of energies is exactly at the orbital on-site energy, α. The red dashed line represents the Fermi level.

It can be seen that the density of states is not as simple as in the equidistant configuration [Fig. 4]. The DOS shows two absolute maxima at Γ, and two local maxima at $\pm$ X. The main difference is that, in the absence of dimerization, the electronic bands at the Fermi level show the largest gradient, and consequently, the lowest DOS. When the system dimerizes and a gap opens at $k = k_{\mathrm{F}}$, the bands flatten around that region, and therefore the density of states increases. However, it is lower than the DOS at Γ. In this case, the density of states is not defined in the region $(-2\delta, 2\delta)$, due to the gap. Consequently, the DOS is not defined at the Fermi level. Besides, it remains approximately constant in the regions $(-2|\gamma|,\ -2\delta)$ and $(2\delta,\ 2|\gamma|)$, where the electronic bands show the greatest gradient.

2.3 Elastic energy of a one-dimensional monoatomic chain

2.3.1 Elastic energy per unit cell in the absence of dimerization

We shall consider the most simple model possible, which consists in a set of springs that connect each atom of the chain with its adjacent ones, all springs being exactly the same, i.e. each spring has the same exact natural length and elastic constant. Under this circumstances, since the system is in its ground state, meaning there are not thermal vibrations of the ions nor the electrons, the nuclei will locate minimizing the elastic potential energy of the system. This results in every spring being in its natural length, which would be the lattice parameter, a, so that the elastic energy is exactly zero.

2.3.2 Elastic energy per unit cell of the dimerized chain

Let us assume the most simple scenario, where only longitudinal movements of the atoms are allowed. In other words, the motion of the atoms is directed along the chain axis. The mechanical collective distortions of the system, which result from the displacement of the atoms departing from their equilibrium positions, shall be modelled with phonons.

Within this model and the configuration sketched in Fig. 1, the maximum displacement in real space of an atom within unit cell m due to a phonon at k is

$$Q(k, T) = Q_0 e^{ikmT}, \tag{70}$$

where Q_0 is the amplitude of the oscillation and T is a translation vector of the Bravais lattice.

Taking into account that $T = a$, the dimerization of the undistorted chain can be described by a phonon at $k = \frac{\pi}{a}$, since

$$Q\left(\frac{\pi}{a}, T\right) = Q_0 e^{im\pi}, \tag{71}$$

where it can be seen that, for each atom, the displacement is antiparallel to that of its adjacents. This deformation is illustrated in Fig. 12.

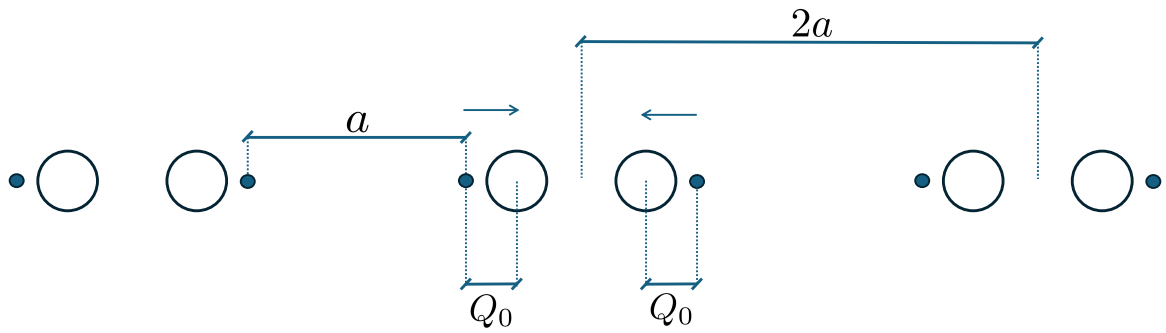

Figure 12: Sketch of a dimerized linear chain with each atom departing a distance Q_0 from its original equilibrium position.

Making use of the harmonic approximation, it is possible to obtain the dispersion relation, i.e. the angular frequency of the motion of the atoms as a function of the wave-vector, ω_k, in a monoatomic chain with lattice parameter a and one atom per unit cell [21],

$$\omega_k = \sqrt{\frac{4C}{M}} \left| \sin\left(\frac{ka}{2}\right) \right|, \tag{72}$$

where C is the elastic constant between nearest neighbours and M is the mass of the atoms of the chain.

Since the phonon is at $k = \pi/a$, the angular frequency of the oscillation is

$$\omega_{\pi/a} = \sqrt{\frac{4C}{M}}. \tag{73}$$

In the dimerized state, the system is composed of two atoms of mass M per unit cell, each in the highest potential energy configuration of a simple harmonic motion, which is described by the phonon. The angular frequency in this kind of oscillation is

$$\omega_{\text{SHM}} = \sqrt{\frac{K}{m}}, \tag{74}$$

where K is the force constant that characterizes the motion and m is the mass of the oscillator.

The potential energy of a harmonic oscillator is

$$U_{\text{SHM}} = \frac{1}{2} K u^2, \tag{75}$$

where u is the displacement of the mass from the equilibrium point. Taking into account the relation between K and ω_{SHM} [Eq. (74)], the potential energy [Eq. (75)] can be expressed as

$$U_{\text{SHM}} = \frac{1}{2} \cdot m \cdot \omega_{\text{SHM}}^2 \cdot u^2. \tag{76}$$

Finally, one can particularize for the dimerized chain by setting $m = M$, $u = Q$, $\omega_{\text{SHM}} = \omega_{\pi/a}$, therefore obtaining the elastic energy per unit cell of the dimerized state,

$$\begin{aligned} E_{\text{elastic}}^{\text{dim}} &= 2 \cdot \frac{1}{2} \cdot M \cdot \frac{4C}{M} \cdot Q^2 \\ &= 4CQ^2, \end{aligned} \tag{77}$$

where the factor of 2 is to account for both atoms of the unit cell.

2.4 Stability of the dimerized chain

To determine whether the system is more stable when it dimerizes, it is necessary to compute the total energy variation. The elastic energy variation per unit cell is

$$\Delta E_{\text{elastic}} = E_{\text{elastic}}^{\text{dim}} - E_{\text{elastic}}^{\text{non dim}}, \tag{78}$$

where $E_{\text{elastic}}^{\text{dim}}$ is the elastic energy per unit cell of the dimerized system [Eq. (77)], and $E_{\text{elastic}}^{\text{non dim}}$ is the same quantity in the absence of dimerization, whose value was deduced in Sec. 2.3.1. Replacing this values in Eq. (78), the elastic energy variation per unit cell results

$$\Delta E_{\text{elastic}} = 4CQ^2. \tag{79}$$

On the other hand, to determine the variation in electronic energy per unit cell, one can simply multiply the electrostatic energy variation per unit length deduced in Sec. 2.2.3 [Eq. (61)], by a factor of $2a$, which is the length of the unit cell in the dimerized system, obtaining

$$\begin{aligned}\Delta E_{\text{elec}} &= 2a \cdot \frac{4\gamma}{\pi a} \cdot \lambda \left[0.443 - \frac{1}{4}\ln(\lambda)\right] \\ &= \frac{8\gamma}{\pi}\lambda \left[0.443 - \frac{1}{4}\ln(\lambda)\right].\end{aligned} \tag{80}$$

Thus, the total energy variation results

$$\begin{aligned}\Delta E &= \Delta E_{\text{elec}} + \Delta E_{\text{elast}} \\ &= \frac{8\gamma}{\pi}\lambda \left[0.443 - \frac{1}{4}\ln(\lambda)\right] + 4CQ^2.\end{aligned} \tag{81}$$

In order to approach this variation from an analytical point of view, we shall consider that the electron-lattice coupling is governed by a linear law, i.e. there is a linear dependency between the hopping term correction, δ, and the distance that the atoms displace from their equilibrium points, Q. That is,

$$\delta \propto Q. \tag{82}$$

When the system dimerizes, the distance between atoms departs from the equilibrium distance, a. In the dimerized system, there will be a short and a long bond, whose lengths amount to $a - 2Q$ and $a + 2Q$, respectively. Thus, for convenience, it is possible to set that the dependency is

$$\delta = \eta \cdot 2Q, \tag{83}$$

where η is the electron-lattice coupling constant. Given that by definition $\delta \geq 0$, η and Q will be both defined non-negative as well. The electron-lattice coupling constant accounts for the rate of change of the hopping parameter between two adjacent atoms when one of them shifts along the longitudinal axis of the chain.

Introducing this dependency in the total energy variation [Eq. (81)], and remembering that $\lambda = \frac{\delta^2}{\gamma^2}$,

$$\begin{aligned}\Delta E &= \frac{8}{\pi\gamma}\delta^2 \left[0.443 - \frac{1}{4}\ln\left(\frac{\delta^2}{\gamma^2}\right)\right] + 4CQ^2 \\ &= \frac{32\eta^2}{\pi\gamma}Q^2 \left[0.443 - \frac{1}{4}\ln\left(\frac{4\eta^2}{\gamma^2}Q^2\right)\right] + 4CQ^2.\end{aligned} \tag{84}$$

The total energy variation of the system [Eq. (84)] is a function of the displacement of the atoms, Q, and depends on three parameters: the electron-lattice coupling constant, η, the hopping parameter, γ, and the elastic constant of the system, C. This equation contains an approximation of the complete elliptic integral of the second kind [Eq. (60)], whose relative error increases with λ. According to the electron-lattice coupling law [Eq. (83)], this parameter increases with δ, that accounts for the amount of dimerization. As the system dimerizes, λ becomes larger, resulting in a greater energy variation error. Nevertheless, the maximum possible value is $\lambda = 1$, where the relative error reaches approximately 8%. This is acceptable, since it is likely being outweighed by other approximations considered, such as nearest-neighbor interactions, the exclusion of anharmonic terms in lattice interactions, and non-overlapping orbitals.

We shall delve into the characteristics of the total energy variation:

- Note that $Q = 0$ is not in the domain of the function, since the elliptic integral from Eq. (59) has no real solutions for $\lambda = 0$. Although, $Q = 0$ corresponds to the no-dimerization case, and it can be seen that

$$\lim_{Q\to 0} \Delta E = 0, \tag{85}$$

  since the divergence of the natural logarithm is mitigated by Q^2. Consequently, for convenience, we will consider that $Q = 0$ is inside the domain of the function, and set $\Delta E(Q = 0) = 0$.

- The total energy variation is symmetric with respect to the origin. As deduced from the effect of the phonon at $k = \frac{\pi}{a}$ [Eq. (71)], the dimerization of the system for negative values of Q is fundamentally identical to that for positive values. The only difference lies in the direction of the atomic displacements: atoms move oppositely for negative Q compared to positive Q. However, it does not affect the intrinsic properties of the system.

- The total energy variation is described by a C^1 function, meaning that only its first derivative is continuous across the entire domain. Higher-order derivatives contain terms involving natural logarithms whose divergences are not mitigated by the polynomial terms in Q. As a result, these higher-order derivatives are non-defined at $Q = 0$.

In order to study the stability of the dimerized chain, we need to analyze the critical points of the total energy variation. For convenience, we will rename $\alpha = \frac{32\eta^2}{\pi\gamma}$ and $\beta^2 = \frac{4\eta^2}{\gamma^2}$ and rearrange the terms in Eq. (84),

$$\begin{aligned}\Delta E &= \alpha Q^2 \left[0.443 - \frac{1}{4}\ln\left(\beta^2 Q^2\right)\right] + 4CQ^2 \\ &= Q^2\left[0.443\alpha + 4C - \frac{1}{2}\alpha\ln\left(|\beta Q|\right)\right].\end{aligned} \tag{86}$$

Therefore, the first derivative of the total energy variation:

$$\begin{aligned}\frac{\mathrm{d}\left(\Delta E\right)}{\mathrm{d}Q} &= Q\Big[0.886\alpha + 8C - \alpha\ln\left(|\beta Q|\right)\Big] - \frac{1}{2}\alpha Q \\ &= Q\Big[0.386\alpha + 8C - \alpha\ln\left(|\beta Q|\right)\Big] \\ &= \alpha Q\Big[0.386 + \frac{8C}{\alpha} - \ln\left(|\beta Q|\right)\Big].\end{aligned} \tag{87}$$

In order to find the critical points of the function, we set $\frac{d(\Delta E)}{dQ} = 0$,

$$\begin{aligned}0 &= \alpha Q\Big[0.386 + \frac{8C}{\alpha} - \ln\left(|\beta Q|\right)\Big] \\ &\implies \begin{cases} Q_0 = 0 \\ Q_* = \pm\frac{1}{\beta}\left(e^{0.386}\cdot e^{\frac{8C}{\alpha}}\right)\end{cases},\end{aligned} \tag{88}$$

where it can be seen that there are three critical points. To determine whether they are maxima or minima, we need to compute the second derivative of the total energy variation,

$$\begin{aligned}\frac{\mathrm{d}^2\left(\Delta E\right)}{\mathrm{d}Q^2} &= \alpha\Big[0.386 + \frac{8C}{\alpha} - \ln\left(|\beta Q|\right)\Big] - \alpha \\ &= \alpha\Big[-0.614 - \ln\left(|\beta Q|\right)\Big] + 8C \\ &= |\alpha|\Big[0.614 + \ln\left(|\beta Q|\right)\Big] + 8C,\end{aligned} \tag{89}$$

where it has been taken into account that $\alpha < 0$, and therefore $\frac{|\alpha|}{\alpha} = -1$.

Regarding the critical points at $Q = \pm Q_*$,

$$\begin{aligned}\left.\frac{\mathrm{d}^2(\Delta E)}{\mathrm{d}Q^2}\right|_{Q=\pm Q_*} &= |\alpha|\left[0.614 + \ln\left(e^{0.386}\cdot e^{\frac{8C}{\alpha}}\right)\right] + 8C \\ &= |\alpha|\left[0.614 + 0.386 + \frac{8C}{\alpha}\right] + 8C \\ &= |\alpha| + \frac{|\alpha|}{\alpha}8C + 8C \\ &= |\alpha| - 8C + 8C \\ &= |\alpha|. \end{aligned} \tag{90}$$

Thus, these critical points are always minima, given that the second derivative of the total energy variation is positive at $Q = \pm Q_*$, regardless of the electronic and elastic parameters of the system.

To determine whether the critical point at $Q = 0$ is a maximum or a minimum, we cannot simply evaluate the sign of the second derivative at that point since it is undefined. Therefore, we must qualitatively analyze the sign of the second derivative as Q approaches 0. Under these circumstances, the natural logarithm takes negative values with module greater than 0.614 due to its asymptotic behavior at $Q = 0$. Consequently, the term $|\alpha|\left[0.614 + \ln\left(|\beta Q|\right)\right]$, governed by the electronic component of the system, will be negative. On the other hand, since $C > 0$, the term $8C$, governed by the lattice component, will always be positive. This is the expected behaviour: given that we are working in the harmonic regime (i.e. no anharmonic terms are being considered in the lattice component of the system, Sec. 2.3), the equidistant configuration is the one with minimal stress. Therefore, any deformation leads to an increase in energy from the lattice point of view. Conversely, as seen in Sec. 2.2.3 [Eq. (61)], any dimerization reduces the electronic energy of the system.

One could expect the sign of the second derivative of the total energy variation to be determined by the interplay between the electronic and lattice components of the system. Nevertheless, given the asymptotic behaviour of the electronic contribution when Q approaches 0, this term will always predominate, independently of the elastic constant of the system. Thus, $\left.\frac{\mathrm{d}^2(\Delta E)}{\mathrm{d}Q^2}\right|_{Q\to 0} < 0 \quad \forall\, \gamma, \eta, C$. Consequently, the equidistant configuration of the chain is always a metastable state, since the total variation of energy [Eq. (84)] exhibits a local maximum at $Q = 0$, as stated by the Peierls' theorem.

The system will always transition to the dimerized state, which has a lower total energy. The energy gain of the system due to dimerization is the minimum of the total energy variation. It can be computed introducing Q_* [Eq. (88)] in the total energy variation [Eq. (84)]. Remembering that $\alpha = \frac{32\eta^2}{\pi\gamma}$ and $\beta = \frac{4\eta^2}{\gamma^2}$,

$$\begin{aligned}\Delta E_{\min} &= \alpha Q_*^2\left[0.443 - \frac{1}{2}\ln\left(|\beta Q_*|\right)\right] + 4CQ_*^2 \\ &= \alpha Q_*^2\left[0.443 + \frac{4C}{\alpha} - \frac{1}{2}\ln\left(|\beta Q_*|\right)\right] \\ &= \frac{\alpha}{\beta^2}e^{0.772}\, e^{\frac{16C}{\alpha}}\left[0.443 + \frac{4C}{\alpha} - \frac{1}{2}\ln\left(e^{0.386}e^{\frac{8C}{\alpha}}\right)\right] \\ &= \frac{\alpha}{\beta^2}e^{0.772}\, e^{\frac{16C}{\alpha}}\left[0.443 + \frac{4C}{\alpha} - \frac{1}{2}\left(0.386 + \frac{8C}{\alpha}\right)\right] \\ &= \frac{\alpha}{\beta^2}e^{0.772}\, e^{\frac{16C}{\alpha}}\left[0.443 + \frac{4C}{\alpha} - 0.193 - \frac{4C}{\alpha}\right] \\ &= \frac{\alpha}{4\beta^2}e^{0.772}\, e^{\frac{16C}{\alpha}} \\ &= -\xi_1|\gamma|e^{-\frac{\pi|\gamma|C}{2\eta^2}}, \quad \text{with} \;\; \xi_1 = 1.378, \end{aligned} \tag{91}$$

which is always negative. This is consistent with the previous analysis, since

$$\Delta E_{\min} < 0 \implies \left.E_{\text{total}}^{\text{dim}}\right|_{Q=\pm Q_*} < E_{\text{total}}^{\text{non dim}}. \tag{92}$$

Qualitatively, one would expect that, for elastically rigid systems with minimal electronic contribution ($C \uparrow$, $|\gamma| \uparrow$, $\eta \downarrow$), the energy gain tends to decrease. The opposite would occur for electronically dominant and elastically soft systems ($C \downarrow$, $|\gamma| \downarrow$, $\eta \uparrow$).

Regarding the value of the displacement of each atom,

$$\begin{aligned} Q_* &= \pm\frac{1}{\beta}\left(e^{0.386}e^{\frac{8C}{\alpha}}\right) \\ &= \pm\,\xi_2\frac{|\gamma|}{\eta}e^{-\frac{\pi|\gamma|C}{4\eta^2}}, \quad \text{with} \quad \xi_2 = 0.736, \end{aligned} \tag{93}$$

this quantity approaches 0 as C increases, for constant values of γ and η. As the elastic interatomic forces become stronger, the extent of dimerization diminishes, although some degree of dimerization always occurs, as deduced. The total energy variation as a function of Q is shown in Fig. 13 for fixed γ and η and different values of C. Additionally, a zoom of the $Q \sim 0$ region is shown on the right side.

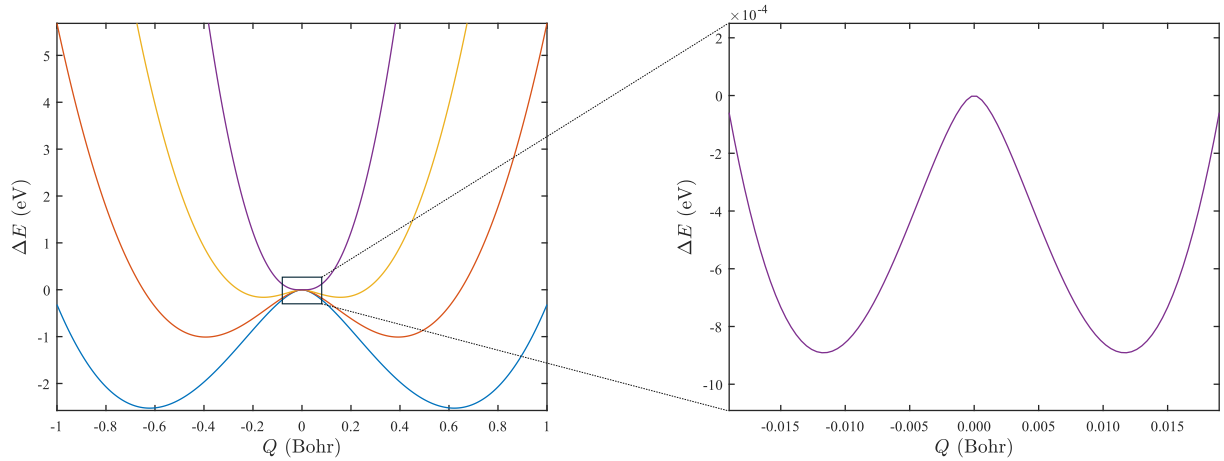

Figure 13: Total variation of energy [Eq. (84)] as a function of Q for $\gamma = -6$ eV, $\eta = 4$ eV/Bohr, $C = 2$ eV/Bohr^2 (blue line), $C = 3.5$ eV/Bohr^2 (red line), $C = 6.5$ eV/Bohr^2 (yellow line) and $C = 15$ eV/Bohr^2 (purple line). A zoom of the $Q \sim 0$ region is shown, where the minima of the purple curve can be observed.

Figure 13 illustrates the previously discussed characteristics of the function that describes the total energy variation of the system. In the left panel, it is evident that for $C = 2$ eV/Bohr^2, $C = 3.5$ eV/Bohr^2, and $C = 6.5$ eV/Bohr^2, the minima are appreciable within the chosen Q scale. Nevertheless, for $C = 15$ eV/Bohr^2, the function apparently does not exhibit minima and resembles a quartic function with its minimum at $Q = 0$. However, by reducing the Q scale and focusing on the $Q \sim 0$ region, the minima in the energy variation become clearly observable, as expected from the previous analysis.

As shown in Fig. 13, for large values of the spring constant C, the distortion that minimizes the energy, Q_*, is small and the double well is very swallow. From a purely theoretical and ideal perspective, as is the case in this study, where it has been assumed throughout that the system is at $T = 0$ (zero temperature), this is not problematic. However, when translating the system to reality, where $T > 0$, thermal vibrations may play a relevant role. In these elastically rigid linear chains, the temperature may be such that thermal vibrations themselves cause the atoms to depart from their equilibrium points and constantly oscillate between $Q = -Q_*$ and $Q = +Q_*$. Thus, by averaging the system's dynamics, it is determined that its stable equilibrium position would be $Q = 0$ rather than $Q = \pm Q_*$. Hence, it can be said that, although the Peierls' theorem has been proven, as expected, it holds true only under ideal conditions, and in reality, there exists a certain limit associated with the elastic rigidity of the system and its temperature. The Peierls distortion, and therefore, the metal-insulator transition, is expected to take place under a certain temperature threshold.

From Fig. 14 to Fig. 19, three pairs of heatmaps are presented. Each pair consists of two heatmaps showing the minimum of the total energy variation, i.e. the energy gain of the system due to dimerization [Eq. (91)], and the corresponding value of Q_* [Eq. (88)], respectively. In each pair, one parameter is fixed while the other two are varied. The marked point corresponds to the set of parameters obtained via first-principles simulations using SIESTA [how to compare the parameters obtained from first-principles with the ones used in the simplified tight-binding model will be discussed in Sec. 3].

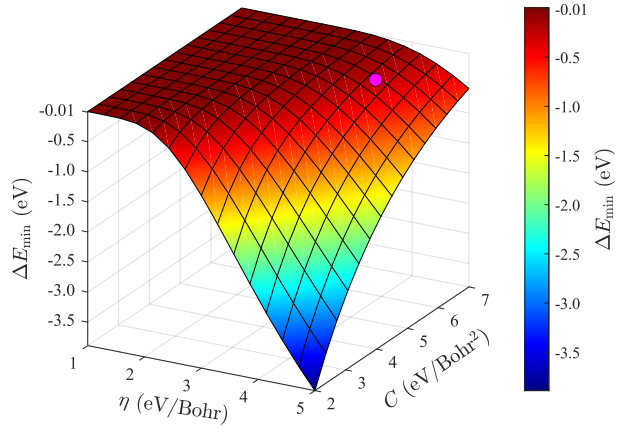

Figure 14: Minimum of the total energy variation as a function of η and C, with $\gamma = -6$ eV.

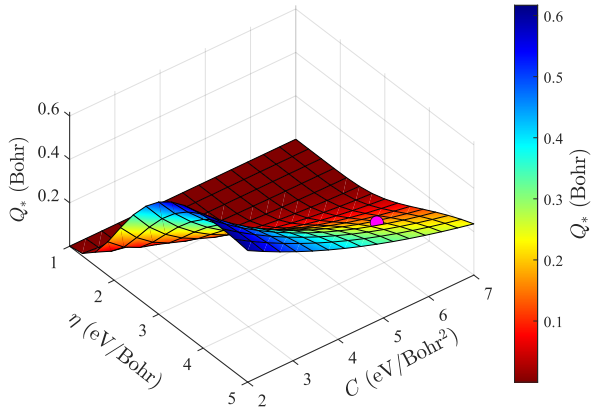

Figure 15: Value of Q_* as a function of η and C, with $\gamma = -6$ eV.

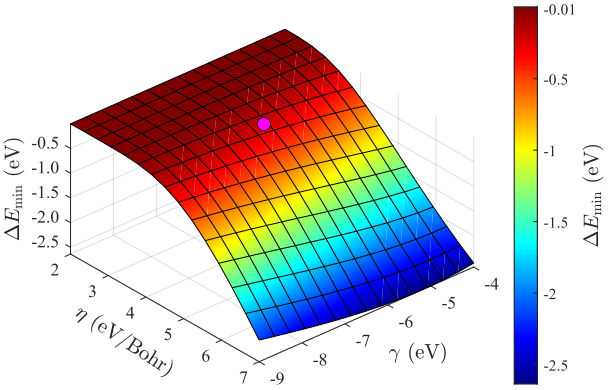

Figure 16: Minimum of the total energy variation as a function of η and γ, with $C = 6$ eV/Bohr^2.

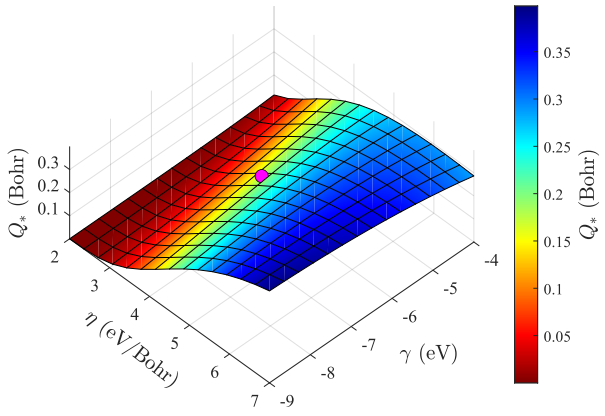

Figure 17: Value of Q_* as a function of η and γ, with $C = 6$ eV/Bohr^2.

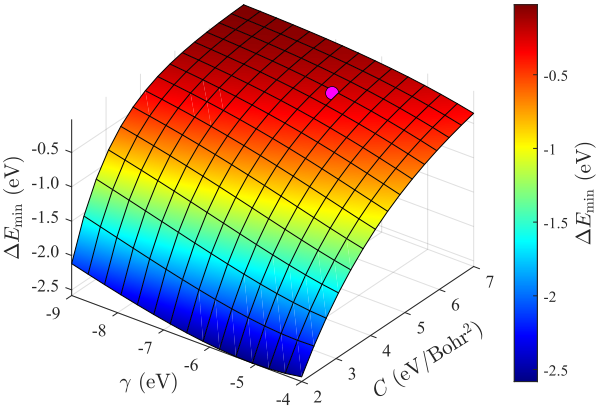

Figure 18: Minimum of the total energy variation as a function of γ and C, with $\eta = 4$ eV/Bohr.

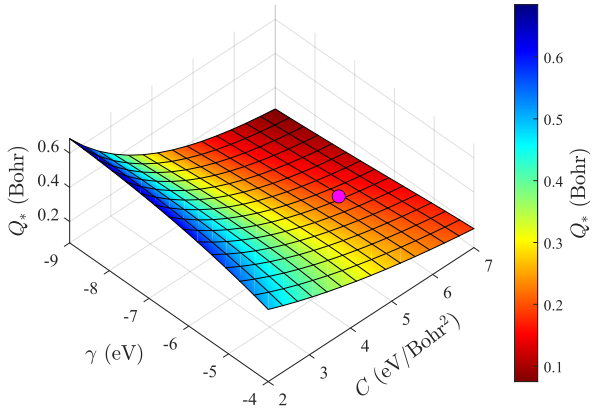

Figure 19: Value of Q_* as a function of γ and C, with $\eta = 4$ eV/Bohr.

In Figures 14 and 15, it can be observed that the characteristics of dimerization exhibit a strong dependence on η and C. For $\eta \uparrow$ and $C \downarrow$, the dimerization is highly prominent, resulting in a significant energy gain and

a large displacement of each atom. In the region where $\eta \downarrow$ and $C \uparrow$, dimerization is practically negligible, though not zero, as it has been demonstrated that dimerization always occurs, however slight it may be.

In Figures 16 and 17, the dimerization shows a stronger dependence on η than on γ, considering that the variation in its characteristics over the γ range is considerably smoother. In the region $\eta \uparrow$, dimerization is very pronounced, in contrast to the region with $\eta \downarrow$, where dimerization is almost negligible. Besides, it can be seen that for $|\gamma| \downarrow$, dimerization is more prominent than for $|\gamma| \uparrow$.

Finally, in Figures 18 and 19, it can be seen that the dependency is mainly on the elastic constant C. For $C \uparrow$ and $|\gamma| \uparrow$ the dimerization essentially dissapears, although for $|\gamma| \uparrow$ it rises considerably. For $C \downarrow$, the dimerization is quite substantial, specially for $|\gamma| \downarrow$.

From the different heatmaps, we can deduce that electronically dominant systems are the ones with $\eta \uparrow$, $|\gamma| \downarrow$ and $C \downarrow$, and elastically dominant systems have $\eta \downarrow$, $|\gamma| \uparrow$, $C \uparrow$. This is consistent with the qualitative analysis performed previously.

Gap opening due to dimerization

As deduced in Sec. 2.2.3, the dimerization of the system leads to the to the opening of a gap at the zone edge with amplitude

$$E_{\text{gap}} = 4|\delta|. \tag{94}$$

The gap, under the established conditions, is direct, meaning the maximum of the valence band and the minimum of the conduction band take place at the same wave-vector, $k = \text{X} = \pi/2a$. This will not be affected by the parameters γ, δ, C. However, the amplitude of the gap, which characterizes the conductivity of the dimerized system, is strongly tied to these magnitudes.

Considering the linear law that governs the electron-lattice coupling [Eq. (83)] and the distance each atom displace from its original equilibrium point, the amplitude of the gap can be expressed as

$$\begin{aligned} E_{\text{gap}} &= 4|\delta| \\ &= 4 \cdot |2\eta Q_*| \\ &= 4 \cdot 2\eta \cdot \xi_2 \frac{|\gamma|}{\eta} e^{-\frac{\pi|\gamma|C}{4\eta^2}} \\ &= \xi_3 |\gamma| e^{-\frac{\pi|\gamma|C}{4\eta^2}}, \quad \text{with} \quad \xi_3 = 5.888, \end{aligned} \tag{95}$$

where it can be observed that the gap amplitude is essentially a decreasing exponential function, similar to the energy gain [Eq. (91)] and the displacement of each atom from its equilibrium point [Eq. (93)]. Qualitatively, its behaviour is inferred to be the same: for elastically rigid systems with minimal electronic contribution ($C \uparrow$, $|\gamma| \uparrow$, $\eta \downarrow$), the gap amplitude tends to decrease. Conversely, it increases for electronically dominant and elastically soft systems ($C \downarrow$, $|\gamma| \downarrow$, $\eta \uparrow$). Additionally, as $E_{\text{gap}} > 0 \ \ \forall\, \gamma, \eta, C$, taking into account that the opening of the gap is due to the dimerization, this result is consistent with all the previous analysis: the system always dimerizes. Figures 20, 21, and 22 present heatmaps showing the gap amplitude values, following the same pattern as the previous heatmaps.

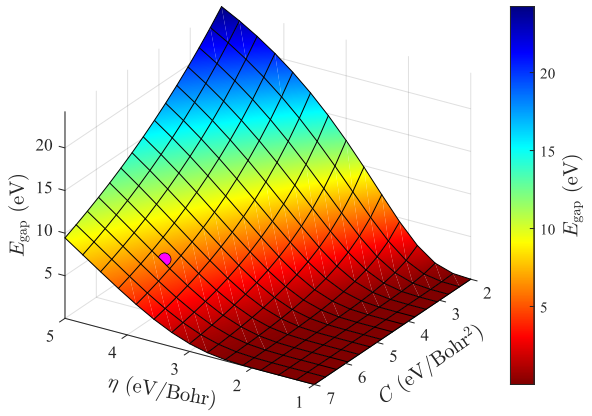

Figure 20: Amplitude of the gap as a function of η and C, with $\gamma = -6$ eV.

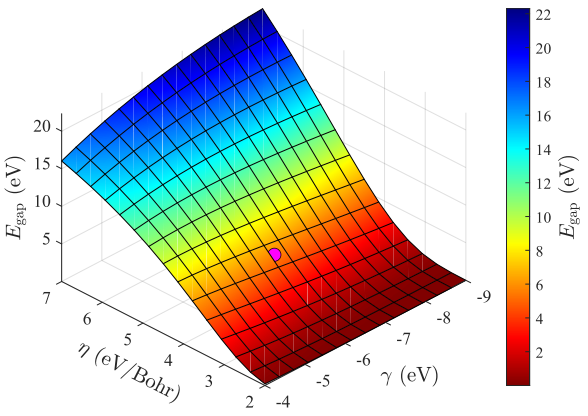

Figure 21: Amplitude of the gap as a function of η and γ, with $C = 6$ eV/Bohr^2.

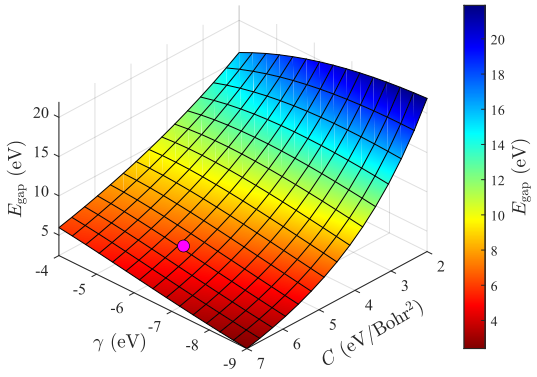

Figure 22: Amplitude of the gap as a function of γ and C, with $\eta = 4$ eV/Bohr.

The heatmaps are qualitatively the same as the ones for $\Delta E_{\min}$ and Q_*, which is reasonable since the functions that describe the amplitude of the gap [Eq. (95)], $\Delta E_{\min}$ [Eq. (91)] and Q_* [Eq. (93)] are similar. In Figures 20 to 22 it can be seen that the amplitude of the gap can reach extremely large values within our analytical model. However, since the typical gap of an insulator ranges from 3 to 7 eV, the regions where the gap is larger are not verisimilar. In Fig. 20, the gap shows such values in the region $\eta \uparrow$ and $C \downarrow$. For $\eta \downarrow$ and $C \uparrow$, the gap amplitude approaches 0. In an intermediate region, where $\eta \sim 1.5$ eV/Bohr and $C \sim 4$ eV/Bohr^2, the gap amounts to around 1 eV, which is the typical gap of an intrinsic semiconductor.

In Figure 21, it can be seen that the dependency of the gap amplitude behaves the same as for $\Delta E_{\min}$ and Q_*. For the region $\eta \sim 2.5$ eV/Bohr, with the given value of C and for every possible γ, the dimerized system would behave like an intrinsic semiconductor. Conversely, for larger values of η, it would be an insulator.

Finally, in Fig. 22, it can be seen that the system would behave like an intrinsic semiconductor in the region $C \sim 7$ eV/Bohr^2 and $\gamma \sim -9$ eV, for the given η. However, for a larger C and lower $|\gamma|$, the gap is large enough to consider it an insulator.

Previously, we discussed that, at sufficiently high temperatures, thermal vibrations could lead to the absence of the metal-insulator transition. In systems where the gap amplitude is small, thermal excitations of the electrons can easily promote them to the conduction band. If the temperature is high enough, a large number of these excitations will take place, and the system will essentially behave like a metal, despite having a non-zero gap. This scenario is analogous to the one discussed earlier: the Peierls transition is expected to occur below a certain temperature threshold.

2.5 The limit of the dimerization

In Sec. 2.2.3, it has been shown that the expression for the energy variation from an electronic perspective [Eq. (61)] is valid solely within the regime $\lambda < 1$. From a purely mathematical viewpoint, this restriction arises due to the fact that the complete elliptic integral of the second kind in Eq. (59) does not have real solutions for $\lambda \geq 1$. The physical significance of this threshold can be understood by examining the definition of this parameter, $\lambda = \frac{\delta^2}{\gamma^2}$, where δ represents the correction of the hopping term: $\gamma - \delta$ for the short bond and $\gamma + \delta$ for the long bond, with $\gamma < 0$ and $\delta > 0$. Recalling the linear law governing the electron-lattice coupling, $\delta = 2\eta Q_*$, where η is the electron-lattice coupling constant and Q_* denotes the displacement of each atom in the stable (dimerized) equilibrium configuration, it can be seen that as the dimerization increases ($Q_* \uparrow$), so does δ. The limit $\lambda = 1$ takes place when $|\delta| = |\gamma|$. In this scenario, the hopping of the short bonds amounts to 2γ, while it reduces to 0 for the long bonds. Thus, there is no electronic interaction between dimers. Consequently, the system essentially consists of a series of Hydrogen molecules that only interact elastically between themselves. The maximum individual displacement of each atom can be deduced by introducing the condition $|\delta| = |\gamma|$ in Eq. (83),

$$Q_*^{\lim} = \frac{|\gamma|}{2\eta}. \tag{96}$$

Besides, note that if $\delta^2 = \gamma^2$, the eigenvalues of the Hamiltonian operator for the dimerized case [Eq. (51)] reduce to

$$\varepsilon_n(k) = \pm 2|\delta| = \pm 2|\gamma|, \tag{97}$$

and the electronic bands are simply two horizontal lines, whose energy difference is exactly $4|\gamma|$ at every wave-vector k.

It is also possible to calculate the energy gain in the limit $\lambda = 1$, by considering this condition and Eq. (96) in Eq. (81):

$$\begin{aligned}
\Delta E_{\min}^{\lim} &= \frac{8\gamma}{\pi}\lambda\left[0.443 - \frac{1}{4}\ln(\lambda)\right] + 4C(Q_*^{\lim})^2 \\
&= 1.128\gamma + 4C\frac{\gamma^2}{4\eta^2} \\
&= 1.128\gamma + C\frac{\gamma^2}{\eta^2} \\
&= \gamma\left(1.128 + C\frac{|\gamma|}{\delta}\right).
\end{aligned} \tag{98}$$

The limit for dimerization encountered in this work is inherent to the employed model. If an alternative model were used, where the modification of the hopping parameter is not linear and, for instance, includes higher-order terms (such as a power series), it is likely that a different limit would be obtained. Intuitively, the physical limit to dimerization would be reached when the individual displacement of each atom results in the dimers being at zero distance from each other, which takes place if

$$Q_* = \frac{a}{2}. \tag{99}$$

Beyond this point, any further increase in displacement would cause the Hydrogen pairs to move apart, effectively reversing the dimerization.

3 First-principles simulations

3.1 What is SIESTA?

SIESTA (Spanish Initiative for Electronic Simulations with Thousands of Atoms) [4] is a method and simulation code for atomic systems (molecules, solids, liquids, surfaces, etc.) that, through the numerical resolution of the quantum-mechanical equations governing the behavior of electrons, allows the determination of atom dynamics and simulation of the physical and chemical processes occurring at the atomic scale. It is based on "first-principles" or "*ab-initio*" methods, particularly on Density Functional Theory (DFT) [22], which does not require prior experimental information. Therefore, it is a method and code of general application not restricted to a specific type of material but can be used to study essentially any system, regardless of its chemical composition or structure.
SIESTA competes with other simulation codes based on DFT. Among them are programs based on plane waves (such as VASP [23], CASTEP [24], or ABINIT [25] among others) or atomic orbitals (such as Gaussian [26] and ADF [27]). Like the latter, SIESTA is also based on the use of atomic orbitals. However, the key to the method's high efficiency lies in the use of numerical atomic orbitals of finite range, whose shape and range flexibility allow optimization of the localization-quality pair. This type of basis also allows the use of the so-called $\mathcal{O}(N)$ methodologies, where calculation time and memory requirements scale linearly with N (the number of atoms) instead of N^3 (as is the case with the other mentioned codes). The efficiency of the methods implemented in SIESTA results in CPU and memory costs much lower than those of other codes. For example, SIESTA can easily handle systems of a few hundred atoms on computers with a single processor, while other codes can only access these sizes when running in parallel. Furthermore, SIESTA's linear scaling ($\mathcal{O}(N)$) makes it possible to address problems with a much higher number of atoms (up to thousands) compared to other codes, which quickly reach the barrier of $\mathcal{O}(N^3)$ scaling. These two characteristics (efficiency and linear scaling with the number of atoms) make SIESTA a unique tool for the atomistic study of complex systems.

3.1.1 Approximations within the first-principles calculations

Essentially, the simulated system remains the same as in the analytical model developed in Sec. 2.2, in particular:

- An infinite linear chain composed Hydrogen atoms.
- One orbital of s-symmetry per site (for the sake of simplicity a minimal basis set is used here).
- One electron per atom.
- At zero temperature.
- The electron will be considered spinless.
- The calculations will always be performed within the Born-Oppenheimer approximations: electrons will be always at their ground state for whatever atomic structure considered (dimerized or not).

However, within our numerical first-principles simulations we go one step-further than in the previous analytical approach in the sense that

- Non-orthogonal atomic orbitals: there is a non-vanishing overlap with neighbour orbitals. That is, $S_{\mu\nu}(|T|>0) = S_{\nu\mu}(|T|>0) \neq 0$.

- At the electronic level, the hopping extends beyond the first-neighbour approximation. Indeed, the basis set in SIESTA is made of strictly localized numerical atomic orbitals, that exactly vanish beyond a given cutoff radius. This cutoff determines the range of the interactions.
- At the lattice level, the interatomic force constants are not restricted to first-neighbours, and anharmonic terms are taken into account.

3.2 Hydrogen chain with one atom per unit cell

The one-dimensional monoatomic chain with a single atom per unit cell cannot exhibit dimerization due to the symmetry constraints inherent in this phenomenon. This configuration, given its intrinsic symmetry, will always have a net force on its atoms equal to zero, but the stress is different from zero, unless the atoms are separated by the equilibrium lattice constant, that can be considered as the natural length in a model of springs. To determine this equilibrium lattice parameter, a structural relaxation will be conducted: the system will be allowed to evolve until the tension on the atoms falls below a specified threshold, set at 0.0001 eV/Å^3. The resulting lattice parameter is

$$a = 2.100 \text{ Bohr}. \tag{100}$$

The Bloch orbitals that describe the electronic density of the system are, by definition, delocalized orbitals. We have performed a Wannierization of the band structure in order to compute the tight binding parameters expressed in a basis of Wannier functions, which are localized. Within our first-principles simulations we have non-null hoppings beyond first-neighbours. To compare with the results shown in Sec. 2.2, we shall report the obtained values for the on-site energy and first-neighbour hopping parameter, which amount to

$$\alpha = -3.106 \text{ eV}, \qquad \gamma = -6.229 \text{ eV}. \tag{101}$$

On the other hand, the energy per unit cell of the equidistant configuration of the monoatomic Hydrogen chain is

$$E_{\text{total}}^{1 \text{ atom/uc}} = -14.750 \text{ eV}, \tag{102}$$

where the superindex accounts for the number of atoms per unit cell.

Regarding the electronic component of the system, in Fig. 23 the band structure of the system is shown, as well as the structure determined using the simplified model [Eq. (22)] using the tight-binding parameters determined computationally [Eq. (101)]. Since the origin of energies is always ill-defined, the Fermi energy of both electronic bands has been set to $E_{\text{F}} = 0$.

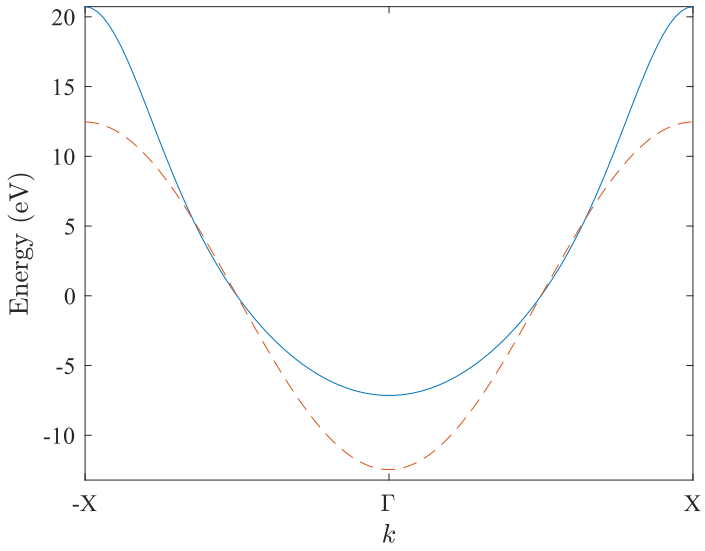

Figure 23: Graphical representation of the electronic energy band for a linear Hydrogen chain with one atom per unit cell obtained using SIESTA (blue solid line) and the eigenvalues of the Hamiltonian operator from the simplified theoretical model [Eq. (22)] determined with the tight binding parameters from SIESTA [Eq. (101)] (red dashed line). The zero of energy corresponds with the Fermi level.

As illustrated in Fig. 23, there are noticeable differences between the band structure obtained from the simplified model and the one derived from first-principles calculations. The main difference is that the lower part of the electronic band obtained from SIESTA (below the Fermi level) is flatter than the one from the theoretical model. Therefore, a larger number of states lie within that k range within $(\varepsilon, \varepsilon + \mathrm{d}\varepsilon)$, and the DOS in that region is higher. Conversely, the part of the band above the Fermi level shows a greater gradient, and therefore, a lower DOS. This will be clearly visible in Sec. 3.3.1. The asymmetry between the electronic band above and below the Fermi level is primarily attributed to the non-orthogonality of the orbitals. As observed in the simplified model, Fig. 2, or particularly in Fig. 6, the electronic bands when the orbitals do not overlap are symmetrical with respect to the Fermi level (where the folding of the bands takes place).

3.3 Hydrogen chain with two atoms per unit cell

3.3.1 No dimerization case

The one-dimensional monoatomic chain with two atoms per unit cell can indeed exhibit dimerization. Initially, first-principles calculations will be conducted for the non-dimerized chain, which corresponds to the basic band model. As the number of atoms per unit cell has been doubled, the lattice parameter is consequently doubled, taking the value

$$b = 2a = 4.200 \text{ Bohr}. \tag{103}$$

The tight binding parameters do not change with respect to the one atom per unit cell case developed in Sec. 3.2. Regarding the total energy of the system, since there are twice the number of atoms per unit cell,

$$E_{\text{total}}^{2\text{ atom/uc}} = 2 \cdot E_{\text{total}}^{1\text{ atom/uc}} = -29.500 \text{ eV}. \tag{104}$$

Left side of Fig. 24 depicts the electronic bands for the non-dimerized case computed with SIESTA, as well as the ones determined with the simplified theoretical model [Eq. (46)], using the tight-binding parameters obtained from first-principles [Eq. (101)]. Right side shows the density of states for the non-dimerized case from first-principles calculations.

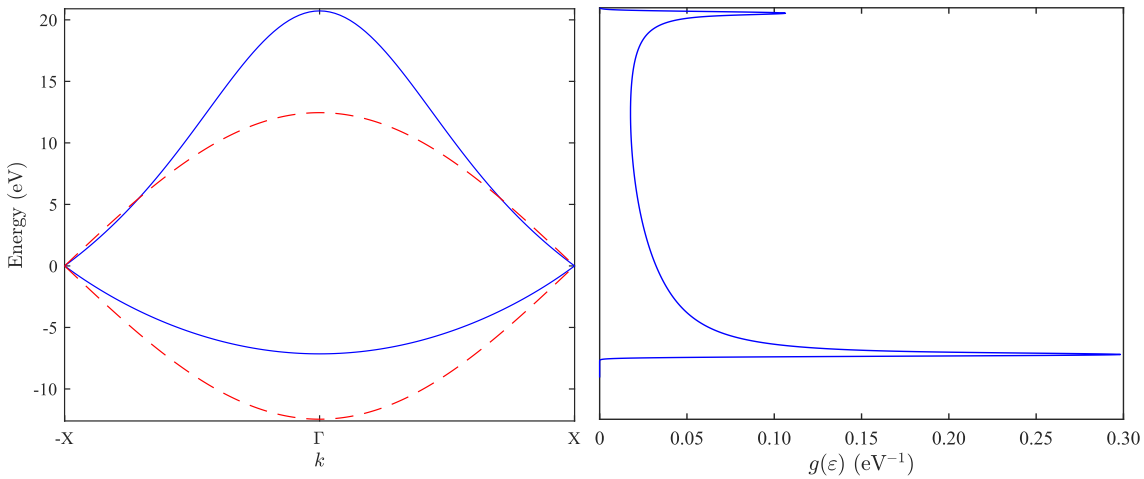

Figure 24: On the left side, the graphical representation of the electronic energy band for a linear Hydrogen chain with two atoms per unit cell obtained using SIESTA (blue solid line) and the eigenvalues of the Hamiltonian operator from the simplified theoretical model [Eq. (46)] determined with the tight binding parameters from SIESTA [Eq. (101)] (red dashed line). The zero of energy corresponds to the Fermi level. On the right side, the density of states obtained from first-principles.

In Figure 24, it is more evident that the basis of atomic orbitals is non-orthogonal, as the asymmetry of the electronic bands determined with SIESTA with respect to the Fermi level is clearly visible. The DOS shows two asymmetrical maxima, both at Γ. The largest density of states corresponds to the lower band, flatter than the upper band. The electronic bands from the theoretical model are symmetrical with respect to the Fermi level, resulting in a symmetric DOS as well [Fig. 4].

3.3.2 Dimerization case

We shall verify whether a monoatomic hydrogen chain at zero temperature spontaneously dimerizes, that is, whether it is unstable with respect to a distortion in real space caused by a phonon at $k = \pi/a$. Essentially, to verify Peierls' theorem. For this purpose, the same chain with two atoms per unit cell as in Section 3.3.1 will be arranged, but with the initial positions slightly displaced. In the non-dimerized case, the atoms are equidistant from each other. Therefore, the first atom of the cell is at $R_1 = 0$, denoting R_1 as the position vector of the ions. The second atom of the cell is at $R_2 = \frac{1}{2}b = a$. To denote this more conveniently, fractional coordinates of the lattice parameter b will be used. In this way, the final configuration of the non-dimerized system is $R = \{0,\ \frac{1}{2}\}$.

To check if the system spontaneously dimerizes, we will set the initial configuration of the atoms as $R_\mathrm{i} = \{0.01,\ 0.49\}$, and we will conduct an structural relaxation, allowing the system to iteratively evolve to its most stable state. The final configuration of the system results

$$R_\mathrm{f} = \{0.050,\ 0.450\}. \tag{105}$$

Where it can be observed that the system has not evolved towards $R_\mathrm{i} = \{0,\ \frac{1}{2}\}$, but has instead acquired a different configuration in which the distance between the atoms in the unit cell is shorter. In the non-dimerized system, distance between atoms is exactly $\frac{1}{2}b = a$. In the dimerized system, the length of the short bond takes the value

$$a - 2Q_* = 0.400b = 1.680\ \text{Bohr}, \tag{106}$$

where the notation from the simplified model has been followed, where Q_* is the individual displacement of each atom from its position in the equidistant configuration, in this case,

$$Q_* = 0.050b = 0.210\ \text{Bohr}, \tag{107}$$

such that $2Q_*$ is the distance they move closer to or farther from their adjacent atoms. Therefore, the length of the long bond amounts to

$$a + 2Q_* = 0.600b = 2.520 \text{ Bohr}. \tag{108}$$

As observed, the system has spontaneously evolved into a dimerized state: the atom at $(\tau_1, T = 0)$ has shifted in the positive direction of the longitudinal axis, while the atom at $(\tau_2, T = 0)$ has moved in the negative direction. Consequently, they have drawn closer to each other, while distancing themselves from the atoms at $(\tau_2, T = -2a)$ and $(\tau_1, T = +2a)$, respectively. This behavior aligns with the predictions of the simplified theoretical model and Peierls' theorem. First-principles calculations predict a dimerization.

The energy of the system when it spontaneously dimerizes, under natural conditions and at zero temperature, takes the value

$$E^{2\text{ atom/uc}}_{\text{total, dim}} = -29.718 \text{ eV}. \tag{109}$$

Thus, the energy gain due to dimerization, using Eq. (109) and (104), takes the value

$$\begin{aligned} \Delta E &= E^{2\text{ atom/uc}}_{\text{total, dim}} - E^{2\text{ atom/uc}}_{\text{total}} \\ &= -0.218 \text{ eV}. \end{aligned} \tag{110}$$

The electronic bands for the dimerized chain are shown on the left side of Fig. 25. On the right side, the density of states for the dimerized case from first-principles.

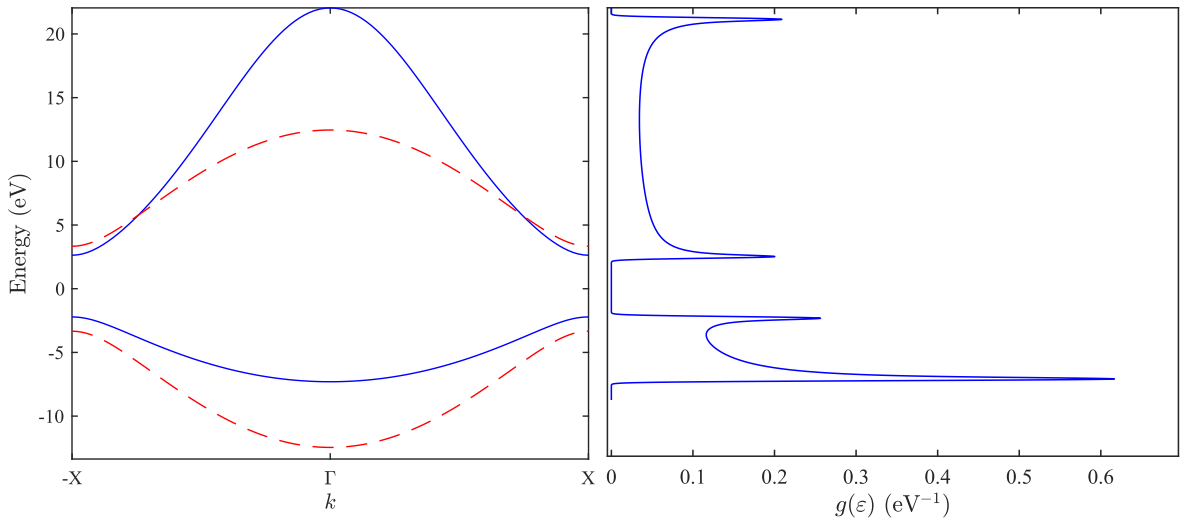

Figure 25: On the left side, the graphical representation of the electronic energy bands for an spontaneously dimerized linear Hydrogen chain with two atoms per unit cell obtained using SIESTA (solid blue line) and the eigenvalues of the Hamiltonian operator from the analytical model [Eq. (52)] determined with the tight binding parameters from SIESTA [Eq. (101), (107) and (112)]. The zero of energy corresponds to the Fermi level. On the right side, the density of states, computed with SIESTA.

Where it can be seen that the electrons with wave-vectors near the Fermi level see their energies lowered, which produces the opening of a gap at the zone edge, whose amplitude amounts to

$$E_{\text{gap}} = 4.842 \text{ eV}, \tag{111}$$

which is large enough to consider the dimerized system an insulator and not an intrinsic semiconductor, whose typical gap is around 1 eV.

Besides, the density of states shows three local maxima and one absolute maximum. The absolute maximum corresponds to the valence band at Γ, the flattest region of the electronic bands. There are two other maxima at the zone edge, where the bands flatten due to the opening of a gap. The DOS at ± X in the valence band

is higher than the one at the conduction band. The last maximum corresponds to the conduction band at Γ, and takes the same value as the one at ± X, meaning that the gradient at Γ and ± X of the conduction band, produced by the opening of the gap, is the same when the chain dimerizes. As expected from the analytical model, the DOS between the valence and conduction bands is null, since there are no states. The main difference is the asymmetry between both bands, which was previously discussed in the no-dimerization case.

The dimerization of the system implies a change in the interatomic distances and, therefore, in the tight-binding parameters. In the simplified theoretical model, it was assumed that there is a linear relation between the hopping parameter correction δ and the individual displacement of each atom, Q_*, which is governed by the electron-lattice coupling constant, η [Eq. (83)]. This coupling is considered, in accordance with the model approximations, only at first neighbours. Nevertheless, in the simulations conducted with SIESTA, the coupling is not restricted to first-neighbours. For comparison, the term that governs the interaction between adjacent atoms is obtained,

$$\eta = 3.971 \text{ eV/Bohr}. \tag{112}$$

Natural elastic constant of the Hydrogen chain

We need to determine the elastic constant that describes the lattice interactions between first-neighbours, decoupled from the electronic component of the system. In order to compute C from first-principles using SIESTA, it is necessary to calculate the phonons of the system, i.e. the dynamic matrix. This procedure is carried out displacing each atom of the Bravais lattice and determining the forces acting on the remaining atoms due to that deformation. The problem is that, for each displacement, the system reaches self-consistency in the electronic component calculations. We are working within the Born-Oppenheimer approximation, i.e. the electrons are always considered to be on their ground-state. As shown, the electrons reach their ground-state through dimerization. Thus, it is impossible to obtain a decoupled elastic constant from the electronic component using this method.

To obtain the elastic constant, we will combine the analytical model and SIESTA. Equation (84) quantifies the energy variation when the system dimerizes as a function of the displacement of each atom, Q, and the parameters γ, η and C. With SIESTA, we have computed the hopping parameter for first neighbours, γ [Eq. (101)], the displacement of each atom when the system reaches its ground-state through dimerization, Q_* [Eq. (107)], the energy gain, ΔE_{min} [Eq. (110)] and the first-neighbours coupling constant, η [Eq. (112)]. It is possible to solve for C in Eq. (84) and introduce the results from SIESTA, obtaining

$$\begin{aligned} C_{\text{natural}} &= \frac{\Delta E_{\text{min}} - \frac{32\eta^2}{\pi\gamma} Q_*^2 \left[0.443 - \frac{1}{4}\ln\left(\frac{4\eta^2}{\gamma^2}Q_*^2\right)\right]}{4Q_*^2} \\ &= 5.867 \text{ eV/Bohr}^2 \end{aligned} \tag{113}$$

which is the decoupled elastic constant that describes the first-neighbours lattice interactions.

Modulation of the transition with an external potential

In SIESTA, it is possible to add an additional term to the Hamiltonian, and therefore subject the system to an external potential. In order to explore the nature of the transition and the interplay between the electronic and elastic components of the monoatomic chain, a harmonic potential will be simulated. Adding a harmonic potential implies modifying the spring constant that characterizes the elastic interaction between the atoms of the lattice. This type of potential is specified by its range of action and the force constant. The new harmonic term will consist of a first-neighbour potential, i.e. with a maximum range of $b = 2a$, so that the net elastic constant of the system, at first-neighbours, for comparison with the simplified theoretical model, is given by

$$C = C_{\text{natural}} + C_{\text{extra}}, \tag{114}$$

The dimerization of the monoatomic Hydrogen chain is simulated for different values of C_{extra}, both positive, increasing the net elastic constant, and negative, decreasing it. Tables 1 and 2 show the values of the energy

gain, ΔE, the displacement of each atom, Q_*, and the gap amplitude, E_{gap}, for different values of C_{extra}, with $C_{\text{extra}} > 0$ and $C_{\text{extra}} < 0$, respectively.

C_{extra} (eV/Bohr^2)	ΔE (eV)	Q_* (Bohr)	E_{gap} (eV)
$+0.5$	-0.143	0.189	4.006
$+1.0$	-0.091	0.159	3.250
$+1.5$	-0.051	0.116	2.588
$+2.0$	-0.035	0.093	2.049
$+2.5$	-0.021	0.074	1.671
$+3.0$	-0.012	0.057	1.242
$+3.5$	-0.007	0.042	0.946
$+7.0$	> -0.001	0.008	0.145

Table 1: Values of the energy gain, ΔE, atom displacements, Q_* and amplitude of the gap, E_{gap}, for different values of an additional positive elastic constant due to an external harmonic potential, C_{extra}, simulated using SIESTA.

C_{extra} (eV/Bohr^2)	ΔE (eV)	Q_* (Bohr)	E_{gap} (eV)
-0.5	-0.324	0.247	5.738
-1.0	-0.466	0.284	6.659
-1.5	-0.648	0.319	7.577
-2.0	-0.874	0.336	8.472
-2.5	-1.145	0.366	9.321
-3.0	-1.461	0.392	9.921
-3.5	-1.821	0.420	10.353
-4.0	-2.224	0.443	10.648

Table 2: Values of the energy gain, ΔE, atom displacements, Q_* and amplitude of the gap, E_{gap}, for different values of an additional negative elastic constant due to an external harmonic potential, C_{extra}, simulated using SIESTA.

Table 1 shows that, as the elastic constant of the system increases due to the external potential, dimerization becomes less pronounced, with the elastic component increasingly dominating over the electronic one. With the natural elastic constant of the system, the energy gain from dimerization amounts to -0.218 eV. However, this gain is nearly halved when the elastic constant is increased by 0.5 eV/Bohr^2, which is just 10% higher than the natural value. The relative variations in the gap amplitude and the displacement of each atom are not as significant as the changes in the energy gain. For high values of the additional elastic constant, dimerization becomes almost negligible, with minimal energy gain, atomic displacement, and gap amplitude. When C_{extra} is approximately 3 eV/Bohr^2, the gap reaches about 1 eV, which is the typical value for an intrinsic semiconductor. For lower elastic constants, the gap is sufficiently large to classify the one-dimensional hydrogen atomic chain as an insulator. Conversely, for higher elastic constants, the gap is small enough for electrons to easily access the conduction band through thermal excitations, meaning that it behaves, essentially, as a metal.

For $C_{\text{extra}} < 0$ [Table 2], where the net elastic constant of the system is lower than the natural one, it can be observed that dimerization becomes more intense as C_{extra} becomes more negative. This is reasonable due to the reduction of the elastic component of the solid with respect to the electronic one. The relative variations in energy gain are not as drastic as in the case of $C_{\text{extra}} > 0$, demonstrating a non-linear behavior, as expected from the analytical model. For highly negative values of the additional elastic constant, or equivalently, for very low values of the net elastic constant, the system achieves significant energy gains, atomic displacements, and gap amplitudes. In the case of $C_{\text{extra}} = -4$ eV/Bohr^2, it is observed that $Q_* = 0.443$ Bohr, indicating that the separation between dimers reaches half of its value without dimerization.

The dynamics of the system obtained from SIESTA does qualitatively match the predicted behaviour of the analytical model. In order to check to what extent the model really adecuates to the simulations, we shall compare both quantitatively.

3.4 Quantitative comparison of the analytical and computational models

With the first-neighbours parameters obtained from the first-principles simulations,

- The hopping term [Eq. (101)], $\gamma = -6.229$ eV,
- The electron-lattice coupling constant [Eq. (112)], $\eta = 3.971$ eV/Bohr,
- The elastic constant (decoupled from the electronic component of the system) [Eq. (113)], $C = 5.867$ eV/Bohr^2,

we shall compare the dimerization characteristics determined with the analytical model developed in Sec. 2.1 and the ones from SIESTA.

The results are shown in Table 3.

	SIESTA	Analytical model	Relative error (%)
ΔE (eV)	-0.218	-0.225	3.2%
Q_* (Bohr)	0.210	0.187	10.95%
E_{gap} (eV)	4.842	5.941	22.7%

Table 3: Values of the energy gain, ΔE, atom displacements, Q_* and amplitude of the gap, E_{gap}, obtained from first-principles simulations and the theoretical analytical model, for the natural one-dimensional monoatomic chain, as well as the relative error.

As it can be observed, the analytical model, despite its simplicity, provides a reasonable approximation to the first-principles calculations. The energy gain shows the smallest relative error, indicating a notably accurate result. However, the accuracy of the model decreases for Q_*, and especially for the gap amplitude. The model predicts higher energy gain and a larger gap compared to the results obtained with SIESTA, despite predicting a smaller individual displacement for each atom. This suggests that the analytical model may overestimate the effects of dimerization, likely due to the electron-lattice coupling law [Eq. (83)] including only a single term. Introducing a more complex law with additional negatively contributing terms might reduce this overestimation, although it would also significantly increase the complexity of the model. Another possibility is that the model underestimates the elastic component of the system. In Sec. 2.3, the harmonic approximation was used. If anharmonic terms had been included in the development of the elastic component, the elastic part might have generally been more dominant. However, once again, the complexity of the model would have increased considerably. Overall, the results are considered acceptable and achieve a good balance between complexity and plausibility.

4 Conclusions

The theoretical analytical model developed in this work goes beyond conventional band theory by incorporating the electron-lattice coupling, enabling the study of the interplay between these two energy components. This approach has confirmed the Peierls theorem: any one-dimensional chain with equidistant atoms is unstable with respect to a lattice deformation that lifts up the degeneracy at the Fermi level. The model includes three fundamental parameters: the hopping term, γ, the electron-lattice coupling constant, η, and the elastic constant of the system, C. It has been demonstrated that the one-dimensional monoatomic chain always undergoes dimerization, regardless of the values of these parameters, and opens a gap at $k = k_{\mathrm{F}}$. The equidistant configuration is always a metastable state. For elastically rigid systems with minimal electronic contribution ($C \uparrow$, $|\gamma| \uparrow$, $\eta \downarrow$), dimerization is practically negligible, but theoretically and ideally, at zero temperature, it always occurs. At non-zero temperatures, thermal vibrations can be such that, on average, the system exhibits an equidistant configuration, thereby setting a physical limit to dimerization related to the temperature of the system. For non-extreme solids, dimerization can reach values such that the system, although it should behave as a metal according to conventional band theory, becomes an intrinsic semiconductor (for mild dimerizations) or, generally, an insulator. The study of the dependencies of the dimerization on the three parameters has also shown that this phenomenon is strongly bounded to η and C, with a lower sensitivity to γ.

On the other hand, a limit in dimerization was found, occurring when the hopping term correction, δ, equals the original parameter, γ. However, this limit is considered intrinsic to the developed model and not a real physical limit. To analyze this, a model of greater complexity and depth would be required, one that considers dimerizations beyond this limit.

In addition to the analytical model, through first-principles atomistic simulations performed with SIESTA, it has been confirmed that the equidistant configuration is unstable, with the system reaching equilibrium when atoms form dimers. Modulating an external potential that modifies the lattice interactions, it has been observed how dimerization increases for electronically predominant systems and decreases for elastically rigid systems, consistent with the results from the analytical theoretical model.

Through these simulations, the hopping term, the electron-lattice coupling constant and the elastic constant, have been obtained. These parameters have been introduced in the analytical model, allowing their comparison. Despite the approximations made in the model, it provides a reasonably faithful representation of the computational results, thus achieving an acceptable balance between complexity and accuracy.

Potential directions and extensions of the work

To continue this work, one of the main possibilities would be to study the limit of dimerization in greater depth. This could be approached in two ways. On one hand, it is possible to modify some of the assumptions of the model, such as the law governing the electron-lattice coupling or the terms considered in the expansion of the system's elastic component. More general coupling laws could be considered, as well as anharmonic terms in the elastic part. On the other hand, it would be possible to study the relation between the Peierls dimerization and temperature, determining to what extent, given a certain temperature, dimerization can be considered as such or, on average, the system oscillates between the equilibrium dimerized configurations and essentially remains in the equidistant configuration.

Another very interesting aspect would be to explore potential practical applications of the Peierls dimerization and the fact that it can be modulated by external potentials. Studying an application that could result in a detector based on this phenomenon would be a very interesting option. Additionally, analyzing a molecule or solid system that exhibits a Peierls transition could help to learn more about this phenomenon and its characteristics.

Another possibility would be to explore applications of the Peierls transition in other areas such as superconductivity, quantum computing, Fermi surface nesting, and other topics of current scientific interest. These fields could greatly benefit from new perspectives and possibilities.

A Approximation: complete elliptic integral of the second kind

In this appendix, we shall obtain the approximation of the complete elliptic integral of the second kind, used in Sec. 2.2.3 [Eq. (60)]. This procedure is based exclusively on the book from Abramowitz, M. and Stegun, I. A., [28]. We begin by recalling the definition of complete elliptic integral of the second kind (page 590, Eq. (17.3.3)),

$$E(z)=\int_0^{\pi/2}\sqrt{1-z\sin^2(\theta)}d\theta. \tag{115}$$

The elliptic integral from Eq. (59) is obtained by setting $z=1-\lambda$. This integral is related to the so-called hypergeometric functions, $F(a,b;c;z)$ (page 591, Eq. (17.3.10)),

$$E(z)=\frac{1}{2}\pi F\left(-\frac{1}{2},\frac{1}{2};1;z\right). \tag{116}$$

To inquire about the hypergeometric functions and its relation with the elliptic integrals, see Chapter 15 from [28]. Nevertheless, the mathematical details are considered to be out of the extent of this work. The F function may be transformed as follows (page 559, Eq. (15.3.11)):

$$\begin{aligned}F(a,b;a+b+m;z)=\ &\frac{\Gamma(m)\Gamma(a+b+m)}{\Gamma(a+m)\Gamma(b+m)}\sum_{n=0}^{m-1}\frac{(a)_n(b)_n}{n!(1-m)_n}(1-z)^n-\\&-\frac{\Gamma(a+b+m)}{\Gamma(a)\Gamma(b)}(z-1)^m\sum_{n=0}^{\infty}\frac{(a+m)_n(b+m)_n}{n!(n+m)!}(1-z)^n[\ln(1-z)-\\&-\psi(n+1)-\psi(n+m+1)+\psi(a+n+m)+\psi(b+n+m)]\\&\text{with}\quad(|\arg(1-z)|<\pi,\ \ |1-z|<1)\,.\end{aligned} \tag{117}$$

where ! denotes the factorial, Γ is the Gamma function, $(a)_n$ and $(b)_n$ are the Pochhamer's Symbols, and ψ is the digamma function, which is the derivative of the neperian logarithm of the Gamma function. We shall set some properties and definitions regarding these:

- Gamma function,

$$\Gamma(1)=1, \tag{118}$$

$$\Gamma\left(\frac{1}{2}\right)=\sqrt{\pi}, \tag{119}$$

$$\Gamma(z+1)=z\Gamma(z). \tag{120}$$

- Pochhamer's Symbols (page 256, Eq. (6.1.22)),

$$(z)_0=1, \tag{121}$$

$$(z)_n=z(z+1)(z+2)...(z+n-1)=\frac{\Gamma(z+n)}{\Gamma(z)}. \tag{122}$$

- Digamma function (page 258, Eqs. (6.3.2), (6.3.3) and (6.3.5)),

$$\psi(1)=-\gamma, \tag{123}$$

$$\psi\left(\frac{1}{2}\right)=-\gamma-2\ln(2), \tag{124}$$

$$\psi(z+1)=\psi(z)+\frac{1}{z}. \tag{125}$$

  where γ is the Euler-Mascheroni constant, whose value is not relevant.

The hypergeometric function needed is the one with set of parameters and variables $\left(-\frac{1}{2},\frac{1}{2};1;1-\lambda\right)$. Therefore, in Eq. (117), we need to set $a=-\frac{1}{2}$, $b=\frac{1}{2}$, $c=1$, $m=c-a-b=1$ and $z=1-\lambda$. Consequently, the first summation in Eq. (117) consists in just the first term, with $n=0$. Regarding the second summation, we neglect terms of order 2 or higher in λ for the approximation. Thus, we shall truncate the series in the first term, which corresponds to $n=0$. Taking this into account in Eq. (117),

$$\begin{aligned}
F\left(-\frac{1}{2},\frac{1}{2};1;1-\lambda\right) &\approx \frac{\Gamma(1)\cdot\Gamma(1)}{\Gamma\left(\frac{1}{2}\right)\cdot\Gamma\left(\frac{3}{2}\right)}\frac{\left(-\frac{1}{2}\right)_0\left(\frac{1}{2}\right)_0}{0!\cdot(0)_0}\cdot\lambda^0+\\
&+\frac{\Gamma(1)}{\Gamma\left(-\frac{1}{2}\right)\cdot\Gamma\left(\frac{1}{2}\right)}\cdot\lambda\cdot\frac{\left(\frac{1}{2}\right)_0\left(\frac{3}{2}\right)_0}{0!\cdot 1!}\cdot\lambda^0\cdot\Big[\ln(\lambda)-\\
&-\psi(1)-\psi(2)+\psi\left(\frac{1}{2}\right)+\psi\left(\frac{3}{2}\right)\Big]\\
&=\frac{2}{\pi}-\frac{1}{2\pi}\lambda\Big[\ln\lambda+\gamma+\gamma-1-\\
&-\gamma-2\ln(2)-\gamma-2\ln(2)+2\Big]\\
&=\frac{2}{\pi}+\frac{1}{2\pi}\lambda\Big[4\ln(2)-1-\ln(\lambda)\Big]. \qquad (126)
\end{aligned}$$

Replacing Eq. (126) in Eq. (116):

$$\begin{aligned}
E(1-\lambda)&\approx 1+\frac{1}{4}\lambda\Big[4\ln(2)-1-\ln(\lambda)\Big]\\
&=1+\lambda\left[\ln(2)-\frac{1}{4}-\frac{1}{4}\ln(\lambda)\right]\\
&=1+\lambda\left[0.443-\frac{1}{4}\ln(\lambda)\right], \qquad (127)
\end{aligned}$$

which is the desired approximation. Note that $z=1-\lambda$ complies with the conditions imposed in Eq. (117). Since $|1-z|<1$, $|\lambda|<1$. Taking into account the definition of λ, $\lambda\equiv\delta^2/\gamma^2$, it must be non-negative if the chain is dimerized, thus, $\lambda<1$. Avoiding negative values of λ is important given that for values $-1<\lambda<0$ the elliptic integral has only imaginary solutions [29]. This can be seen in Eq. (127), since $\ln(\lambda)=\ln(|\lambda|)+i\pi$ if $\lambda<0$. These solutions do not yield any physical meaning.

References

[1] Peierls, S. R. (1971). Bird of Passage: Recollections of a Physicist (Princeton 1985).

[2] Mermin, N. D. (2024). Autobiographical Notes of a Physicist. arXiv (Cornell University). https://doi.org/10.48550/arxiv.2401.04711

[3] International Union of Pure and Applied Chemistry (IUPAC). (2019). Peierls transition. In Compendium of Chemical Terminology (3.0.1). https://doi.org/10.1351/goldbook.p04468

[4] Soler, J. M., Artacho, E., Gale, J. D., García, A., Junquera, J., Ordejón, P., & Sánchez-Portal, D. (2002). The SIESTA method for ab initio order-N materials simulation. Journal of Physics: Condensed Matter, 14(11), 2745. https://doi.org/10.1088/0953-8984/14/11/302

[5] Fernández-Ruiz, T., Sánchez-Movellán, I., García-Lastra, J. M., Moreno, M., Aramburu, J. A., & García-Fernández, P. (2024). Many-body model for the cooperative Jahn-Teller effect in crystals and its associated orbital ordering. Physical Review B, 109(20), 205150. https://link.aps.org/doi/10.1103/PhysRevB.109.205150

[6] I. B. Bersuker, The Jahn-Teller Effect. Cambridge University Press, 2006.

[7] P. García-Fernández, I. B. Bersuker, J. A. Aramburu, M. T. Barriuso, and M. Moreno. (2005). Origin of warping in the $E \otimes e$ Jahn-Teller problem: Quadratic vibronic coupling versus anharmonicity and application to NaCl:Rh2+ and triangular molecules. PHYSICAL REVIEW B 71, 184117. https://doi.org/10.1103/PhysRevB.71.184117

[8] S. Sugano, Y. Tanabe, H. Kamimura, Multiplets of Transition-Metal Ions in Crystals. Academic Press (New York), 1970.

[9] Varignon, J., Bibes, M. & Zunger, A. Origin of band gaps in 3d perovskite oxides. Nat Commun 10, 1658 (2019). https://doi.org/10.1038/s41467-019-09698-6

[10] Sánchez-Movellán, I., Moreno, M., Aramburu, J. A., & García-Fernández, P. (2023). Strain-Induced Ferromagnetic to Antiferromagnetic Crossover in d9-Ion (Cu2+ and Ag2+)-Layered Perovskites. The Journal of Physical Chemistry C, 127(17), 8332-8341. https://doi.org/10.1021/acs.jpcc.3c01166

[11] Liang, S., Bai, Y., & Beng, B. (2006). Peierls instability and persistent current in mesoscopic conducting polymer rings. Physical Review. B, Condensed Matter And Materials Physics, 74(11). https://doi.org/10.1103/physrevb.74.113304

[12] Ahn, J. R., Kang, P. G., Ryang, K. D., & Yeom, H. W. (2005). Coexistence of Two Different Peierls Distortions within an Atomic Scale Wire: Si(553)-Au. Physical Review Letters, 95(19). https://doi.org/10.1103/physrevlett.95.196402

[13] Robert E. Thorne; Charge-Density-Wave Conductors. Physics Today 1 May 1996; 49 (5): 42–47. https://doi.org/10.1063/1.881498

[14] Zhang, B., Zhang, T., Pan, J., Chow, T. P., Aboalsaud, A. M., Lai, Z., & Sheng, P. (2021). Peierls-type metal-insulator transition in carbon nanostructures. Carbon, 172, 106-111. https://doi.org/10.1016/j.carbon.2020.10.037

[15] Xu, W., Leary, E., Sangtarash, S., Jirasek, M., González, M. T., Christensen, K. E., Vicente, L. A., Agraït, N., Higgins, S. J., Nichols, R. J., Lambert, C. J., & Anderson, H. L. (2021). A Peierls Transition in Long Polymethine Molecular Wires: Evolution of Molecular Geometry and Single-Molecule Conductance. Journal Of The American Chemical Society, 143(48), 20472-20481. https://doi.org/10.1021/jacs.1c10747

[16] Streltsov, S. V., Mazin, I. I., Heid, R., & Bohnen, K. (2016). Spin-orbit driven Peierls transition and possible exotic superconductivity in CsW_2O_6. Physical Review. B./Physical Review. B, 94(24). https://doi.org/10.1103/physrevb.94.241101

[17] Andronic, S., & Casian, A. (2017). Metal-Insulator Transition of Peierls Type in Quasi-One-Dimensional Crystals of TTT_2I_3. Advances In Materials Physics And Chemistry, 07(05), 212-222. https://doi.org/10.4236/ampc.2017.75017

[18] Zhang, L., Bhattacharya, U., Bachtold, A. et al. Steady-state Peierls transition in nanotube quantum simulator. npj Quantum Inf 9, 7 (2023). https://doi.org/10.1038/s41534-022-00675-4

[19] Aschroft, N. W., & Mermin, N. D. (1976). Solid State Physics. Saunders College Publishing.

[20] Zheng, Q. (2023, June 6). Peierls transition. Qijing Zheng. http://staff.ustc.edu.cn/∼zqj/posts/Peierls-Transition/

[21] Kittel, C. (1986). Introduction to Solid State Physics. John Wiley & Sons.

[22] Engel, E. (2011). Density functional theory: An Advanced Course. Springer-Verlag Berlin.

[23] Hafner, J. (2008). Ab-initio simulations of materials using VASP: Density-functional theory and beyond. Journal of computational chemistry, 29(13), 2044-2078. https://doi.org/10.1002/jcc.21057

[24] Clark, S. J., Segall, M. D., Pickard, C. J., Hasnip, P. J., Probert, M. I., Refson, K., & Payne, M. C. (2005). First principles methods using CASTEP. Zeitschrift für kristallographie-crystalline materials, 220(5-6), 567-570. https://doi.org/10.1524/zkri.220.5.567.65075

[25] Gonze, X., Amadon, B., Anglade, P. M., Beuken, J. M., Bottin, F., Boulanger, P., ... & Zwanziger, J. W. (2009). ABINIT: First-principles approach to material and nanosystem properties. Computer Physics Communications, 180(12), 2582-2615. https://doi.org/10.1016/j.cpc.2009.07.007

[26] Curtiss, L. A., Redfern, P. C., & Raghavachari, K. (2007). Gaussian-4 theory. The Journal of chemical physics, 126(8). https://doi.org/10.1063/1.2436888

[27] Te Velde, G. T., Bickelhaupt, F. M., Baerends, E. J., Fonseca Guerra, C., van Gisbergen, S. J., Snijders, J. G., & Ziegler, T. (2001). Chemistry with ADF. Journal of Computational Chemistry, 22(9), 931-967. https://doi.org/10.1002/jcc.1056

[28] Abramowitz, M. and Stegun, I.A. (Eds.) (1965) Handbook of Mathematical Functions with Formulas, Graphs, and Mathematical Tables. Dover Publications Inc., New York.

[29] Spanier, J., & Oldham, K. B. (1987). An atlas of functions. Taylor & Francis/Hemisphere.